Tectonic Evolution of the Bristol Bay basin, southeast Bering Sea: Constraints from seismic reflection and potential field data

Kristoffer T. Walker[1] and Susan E. McGeary

Department of Geology, University of Delaware, Newark, Delaware, USA

Simon L. Klemperer

Department of Geophysics, Stanford University, Stanford, California, USA

Received 22 January 2002; revised 19 February 2003; accepted 1 April 2003; published 26 September 2003.

[1] We interpret the tectonic evolution of the Bristol Bay basin, also known as the North Aleutian basin, on the basis of a deep seismic reflection profile, lithologic data from a well, unreversed seismic refraction profiles, a bathymetry profile, a magnetics profile, forward modeling of a gravity profile, and flexural modeling of a basin-wide paleosurface. We present evidence that (1) an early or middle Eocene through late Miocene phase of extension led to fault-controlled subsidence; (2) a late Eocene through early Miocene phase of volcanic-arc loading led to flexural subsidence, which was amplified by additional factors possibly including lithospheric cooling, tectonic compression, reverse or thrust faulting, or small-scale intrusions of dense magma; and (3) a late Miocene through Holocene resurgence of arc volcanism and a northward prograding delta continued (or possibly increased) flexural subsidence in the back arc region. Our interpretations imply that the fault-controlled subsidence in the Bristol Bay basin is genetically linked to that found in the other outer Bering Shelf basins, but the subsequent flexural subsidence of these basins is not related. More fundamentally, our observations suggest that the basin's evolution is unusual and has components typically found in both back arc (extension) and retroarc foreland (flexure) basins. *INDEX TERMS:* 3040 Marine Geology and Geophysics: Plate tectonics (8150, 8155, 8157, 8158); 7205 Seismology: Continental crust (1242); 8105 Tectonophysics: Continental margins and sedimentary basins (1212); 8110 Tectonophysics: Continental tectonics—general (0905); 8120 Tectonophysics: Dynamics of lithosphere and mantle—general; *KEYWORDS:* Bristol Bay Basin, North Aleutian basin, Alaska Peninsula, Aleutian arc, back arc basins, flexure. **Citation:** Walker, K. T., S. E. McGeary, and S. L. Klemperer, Tectonic Evolution of the Bristol Bay basin, southeast Bering Sea: Constraints from seismic reflection and potential field data, *Tectonics*, *22*(5), 1049, doi:10.1029/2002TC001359, 2003.

[1]Now at Stanford University, Stanford, California, USA.

0278-7407/03/2002TC001359$12.00

1. Introduction

[2] The Bristol Bay basin, also known as the North Aleutian basin, is a sedimentary basin in a back arc setting with respect to the Aleutian Arc on the southern Bering continental shelf, Bering Sea (Figure 1). Three different hypotheses seek to explain how and why the Bristol Bay basin formed. *Worrall* [1991] proposes that the Black Hills ridge (Figure 1), or uplift, sits between a left stepping pair of late Eocene-Miocene right-lateral strike-slip faults. He cites elastic dislocation modeling by *Rodgers* [1980], and argues that the Bristol Bay basin is a structural sag—the deflected side of a right-lateral strike-slip fault that separates the basin from the uplifted Black Hills ridge to the southwest (Figure 1). He also interprets antiforms and synforms in the basement topography to be folds associated with latest Eocene-late Pliocene transpression. Worrall's hypothesis requires a temporal correlation between the subsidence of the Bristol Bay basin and the Amak, St. George, Pribilof, and Navarin basins along the outer Bering shelf (Figure 1), because their subsidence would also have been affected by the common strike-slip fault zone that he suggests borders or bisects these outer shelf basins.

[3] *Bond et al.* [1988] argue that the Bristol Bay basin subsided because of flexure in the back arc region, possibly caused by Oligocene-Holocene crustal thickening of the Alaska Peninsula. Since the arc jumped from the outer Bering Shelf margin to its current location along the Aleutian islands around 50 Ma [*Marlow et al.*, 1973; *Scholl et al.*, 1987], this hypothesis implies that the basin-forming mechanism was unique to the Alaska Peninsula region, and not common to all the outer Bering shelf basins. It also implies that Tertiary right-lateral strike-slip faulting along the outer shelf margin (hypothesized by *Worrall* [1991]), had an insignificant effect, if any, on Bristol-Bay-basin subsidence.

[4] A third hypothesis argues that a lithospheric-scale down-to-the-north normal fault separating the Black Hills ridge from the southern boundary of the Bristol Bay basin controls basin subsidence (Figure 1; G. Bond, Columbia University, personal communication, 2003). Consequently, this hypothesis implies that the Bristol Bay basin is simply the subsided hanging wall of a lithospheric-scale half-graben.

[5] In this paper we test between these competing hypotheses by interpreting and modeling various geophysical

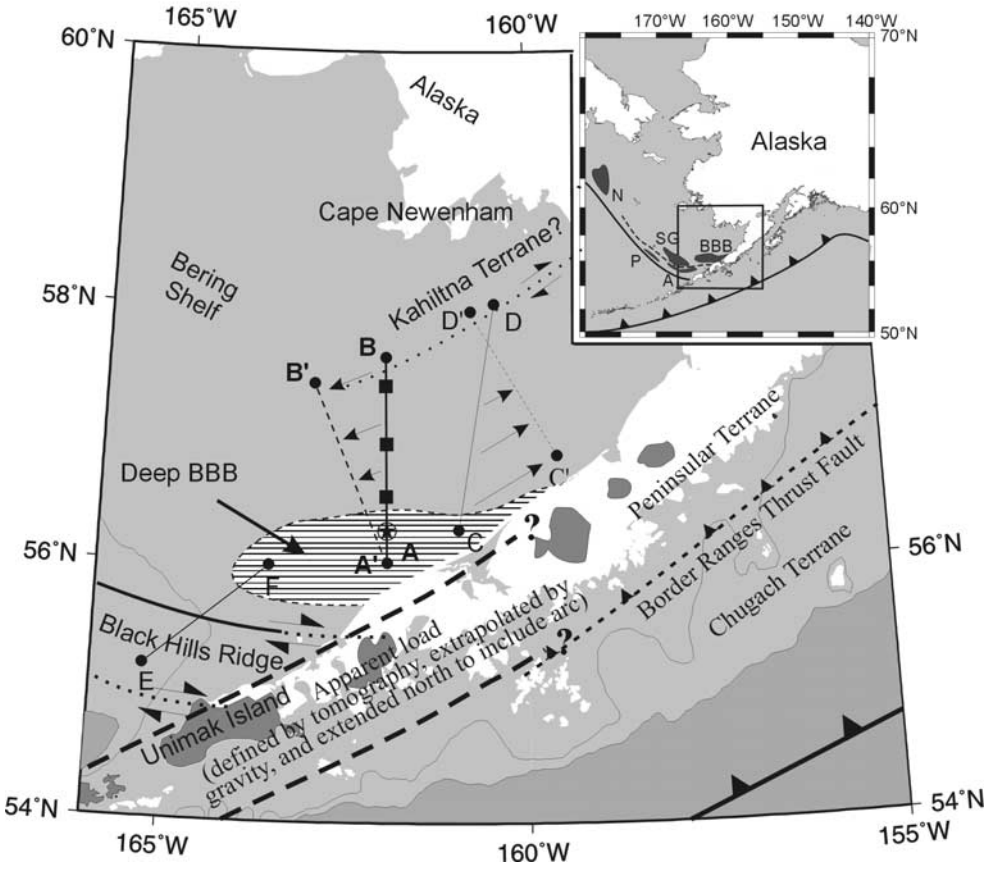

Figure 1. Map of the Bristol Bay basin (also known as the North Aleutian basin) and surrounding region. The boundaries of the Bristol Bay basin (BBB) are hard to define, but the horst and graben part (deep BBB) is roughly identified by the area with horizontal striping to the north of the Alaska Peninsula [*Worrall*, 1991]. Line A–B is the reflection profile presented in this paper. A′–B′ is the line onto which the "red event" was projected for flexural modeling purposes (Figure 8). C–D is the refraction profile, and C′–D′ the projection used by *Bond et al.*'s [1988] flexural modeling. E–F is a deep seismic reflection profile presented by *Lizarralde et al.* [2002]. The Black Hills ridge is bordered by right-lateral wrench faults (dashed lines where inferred) [*Worrall*, 1991; *Lizarralde et al.*, 2002]. The star identifies the COST well [*Turner et al.*, 1988]. Squares represent location of sonobuoys (for long-offset refraction data). Thick dashed lines delineate the apparent load, which is defined by seismic tomography [*Fliedner and Klemperer*, 2000] and extrapolated by gravity [*Barnes et al.*, 1994]. Dark bodies are Quaternary volcanic fields [*Beikman*, 1980]. Thin solid lines represent seafloor depth contours (100 m, 200 m). Light gray shading represents depths <200 m, and deep gray represents depths >200 m. The volcanic arc is built upon the accreted Peninsular terrane, which is separated from the Chugach terrane (forearc) by the inferred extension of the Border Ranges thrust fault. Inset map: Bering Shelf basins from NW to SE are the Navarin (N), Pribilof (P), St. George (SG), Amak (A), and Bristol Bay basin (BBB); the dotted line delineates the axial trace of the Black Hills/Pribilof Ridge [*Marlow et al.*, 1987], and the solid line the inactive Bering Shelf margin.

data sets collected along a basin-crossing profile during the Pacific to Bering Shelf Deep Seismic Experiment. We present evidence that the Bristol Bay basin was created by (1) early or middle Eocene extension, (2) late Eocene to middle Miocene flexural subsidence probably due to several factors, and (3) late Miocene-Holocene flexural subsidence probably associated with renewed volcanism on the Alaska Peninsula and a northward prograding delta. These data suggest that basin subsidence was initiated by extension, probably associated with right-lateral strike-slip faulting similar to that proposed by *Worrall* [1991], then further modified by elements of *Bond et al.*'s [1988] flexural model.

2. Geological Setting

[6] The Bristol Bay basin (BBB) is one of several sedimentary basins located along the margin of the Bering shelf, a large continental shelf about half the size of Alaska

with an average water depth of 150 m (Figure 1). The elongate BBB is located in a back arc setting on the southeastern Bering shelf, and is isolated from the Pacific Ocean by the Alaska Peninsula.

[7] The boundaries of the BBB are not well defined, in part, because the basement depth varies considerably. It is roughly 300 km long parallel to the Peninsula, and is 75 km to roughly 200 km wide [*Marlow et al.*, 1987]. The basin is remarkably asymmetric—it has a maximum basement depth of at least 6 km in the south [*Cooper and Marlow*, 1983; *Marlow et al.*, 1987; *Turner et al.*, 1988; *Marlow et al.*, 1994], and gradually thins to less than 500 m in the north. Sediment provenance studies from three basin wells (2 onshore, 1 offshore) show that the basin fill originated from mostly volcanic rocks, and was deposited in non-marine to shallow marine depositional environments [*Turner et al.*, 1988].

[8] The Alaska Peninsula basement is composed of the Peninsular terrane, an allochthonous mass of mostly arc magmatic rocks that accreted to the margin ~100 Ma b.p. This terrane consists of Upper Triassic to Lower Cretaceous volcanic and volcaniclastic rocks overlying a basement composed of Upper Paleozoic carbonate and schist [*Plafker and Berg*, 1994]. Cenozoic arc volcanism, due to subduction in the south, has covered the Peninsular terrane with additional volcanic and volcaniclastic sedimentary rocks. This ''carapace'' sequence commonly overlies bedrock of the Peninsular terrane throughout the outer Bering shelf [*Worrall*, 1991; *Klemperer et al.*, 2002], and is mostly comprised of non-marine volcaniclastic sedimentary rock ranging from Late Cretaceous to middle Eocene in age [*Worrall*, 1991].

[9] Near the eastern end of the BBB, basement outcrops on the Alaska Peninsula consist of deformed, intruded Mesozoic and older rock [*Hatten*, 1971] of the Peninsular terrane [*Jones and Silberling*, 1979; *Worrall*, 1991]. Outcrops of the southern part of the BBB, exposed along the northern coast of the Alaska Peninsula, are composed of Mesozoic and Cenozoic sedimentary rocks with a volcanic and plutonic provenance [*McLean*, 1977; *Jones and Silberling*, 1979]. *Worrall* [1991] proposes that the southwestern part of the BBB is separated from the offshore extension of the Black Hills ridge by a right-lateral strike-slip fault (Figure 1). The Black Hills ridge, also part of the Peninsular terrane [*Worrall*, 1991], trends along the length of the Alaska Peninsula to Unimak Island, and extends offshore from Unimak along the inside edge of the Bering shelf margin where it is locally called the Pribilof ridge [*Marlow and Cooper*, 1980; *Cooper et al.*, 1987]. In the north, the BBB boundary is not well defined; however, geophysical data suggest that the basement consists of Mesozoic sedimentary, igneous, and metamorphic rock [*Marlow et al.*, 1994]. Since the Peninsular terrane in southern Alaska is bordered to its north by the Kahiltna terrane [*Decker et al.*, 1994], a terrane comprised of highly deformed flysch deposited in a peripheral basin setting prior to the accretion of the Peninsular terrane, the Kahiltna terrane may also extend offshore beneath the Bering shelf and may constitute the shelf basement in the north [*McGeary and Ben-Avraham*, 1981; *Cooper et al.*, 1987; *Marlow et al.*, 1987; *Walker*, 1998].

3. Preexisting Data

[10] During the past 30 years, various geological and geophysical data have been acquired in the Bristol Bay region by petroleum companies and the United States Geological Survey (USGS) [*Cooper et al.*, 1987; *Worrall*, 1991]. These data include mainly upper crustal multichannel seismic reflection profiles and numerous unreversed sonobuoy refraction profiles [*Marlow et al.*, 1977; *Cooper et al.*, 1980; *Marlow and Cooper*, 1980; *Cooper and Marlow*, 1984; *Cooper et al.*, 1987; *Marlow et al.*, 1987], magnetic data [*Pratt et al.*, 1972; *Bailey et al.*, 1976; *Marlow et al.*, 1976; *Childs et al.*, 1981], gravity data [*Childs et al.*, 1985], and depth-to-basement contour maps [*Cooper et al.*, 1979, 1987]. Surface-wave dispersion data have been collected by various authors [*Jin and Herrin*, 1980; *Niazi and Chun*, 1989]. The interpreted geologic history of the Bristol Bay region, based on these data, has been most recently summarized by *Cooper et al.* [1987], *Marlow et al.* [1987], *Worrall* [1991], *Marlow et al.* [1994], and *Plafker and Berg* [1994].

[11] The most relevant stratigraphic data come from a 1982–1983 continental offshore stratigraphic test (COST) well that was drilled to determine the hydrocarbon potential of the Bristol Bay basin [*Turner et al.*, 1988]. The total depth of the well was 5.2 km, and a suite of cores, density logs, and sonic logs were also acquired. These data are used to constrain the ages of the seismic reflectors, and are thus invaluable in establishing the approximate timing of the tectonic events that have shaped the basin.

4. The Pacific to Bering Shelf Deep Seismic Experiment

[12] A deep crustal seismic reflection profile across the BBB, collected in July 1994, was acquired as part of a data set of over 5000 km of seismic reflection data in the Bering Sea region [*McGeary et al.*, 1994]. Sonobuoys, ocean-bottom-seismometer (OBS) arrays, and onland seismometers were also deployed to collect wide-angle reflection/refraction data [*Fliedner and Klemperer*, 1999; *Holbrook et al.*, 1999; *Fliedner and Klemperer*, 2000; *Lizarralde et al.*, 2002]. Bathymetry and potential field data were collected concurrently with the reflection profiles.

[13] The focus of this paper is the southern half (A–B) of one of the marine seismic reflection profiles across the Bering shelf (Figure 1). A–B starts just north of Unimak Island and extends north to about 100 km south of Cape Newenham; it provides a nearly complete transect across the Bristol Bay basin perpendicular to the axis of the basin. The profile also crosses the location of the COST well, where dated unconformities [*Turner et al.*, 1988] can be correlated to reflectors, and extrapolated throughout the reflection profile. Because we analyze several independent sets of data, gleaning pieces of information from each analysis, we

present each data set first, then we synthesize all the information to arrive at a tectonic interpretation.

5. Seismic Reflection Data

[14] The signal-to-noise ratio of the seismic reflection data varied significantly along the profile. The shallow data (0–6 s) are of excellent quality, and contain many reflections of varying amplitude and frequency. Conversely, the deep data (6–16 s) are plagued with high-amplitude coherent noise, and consequently were processed separately.

[15] Standard processing algorithms using ProMAX software were used to process the shallow data. In sequence, these included: a spherical-spreading correction, band-pass filtering (8 Hz at 12 db/oct, 54 Hz at 60 db/oct), F-X deconvolution, predictive deconvolution, velocity analysis (iteratively), NMO correction, 5-trace-mix, a far-offset linearly weighted stack to reduce multiples, predictive deconvolution, Kirchhoff time migration (up to 45° dips), 5-trace-mix, and depth conversion. The depth conversion used the spatially varying interval-velocity profile, which was derived from the final stacking-velocity profile. This processing effectively removed the multiples associated with the basin sediments, improved the lateral resolution of the data, and restored the reflectors to their approximate true spatial position in depth (assuming no out-of-plane reflections).

5.1. Shallow Data Description

[16] The shallow reflection data delineate the stratigraphy and structure across the offshore Bristol Bay basin (Figure 2). On the basis of the relief of the interpreted basement as seen on the seismic profile, and on diffractions observed in unmigrated data, the basin basement shows two distinctly different structural styles separated by ''transition X'' (Figure 2). South of this transition, we interpret the deepest part of the basin to be characterized by fault-bounded horsts and grabens, with structural relief of up to 2–3 km and fairly deep sedimentary reflectors within the grabens. Gravity modeling (below) corroborates our interpretation that these antiforms/synforms are horsts and grabens rather than gentle basement folds as interpreted by *Worrall* [1991]. For convenience, the grabens and half-grabens in the data are named G1–G4 from south to north. Figure 3 shows three of these structures (G1–G3) in more detail. The key observations for our interpretation are the abrupt transition across steep boundaries (faults?) from reflective (sedimentary rocks?) to non-reflective (basement?) regions (Figure 3), and in places, small offsets in reflectors at the inferred fault (e.g., km 50, Figure 2). The basement beneath the horsts and grabens shows only a few sparse chaotic or discontinuous events of variable amplitude and moderate frequency. These events may be weak reflections, or may be residual multiple or diffraction energy.

[17] In contrast, the BBB basement north of transition X exhibits no significant structural relief; the top-of-acoustic-basement reflector (Figure 2) dips gently southward toward the basin axis from the nearly sediment-free region of the inner Bering shelf. The basement in this region is characterized by numerous, although usually discontinuous, events of moderate reflectivity and low-to-moderate frequency. These events usually have shallow dips, and appear to be truncated at the basin/basement interface. Some of the more continuous, horizontal events beneath 0.75-km depth from km 140–174 may be interlayer multiples not attenuated during processing.

[18] The prominent, laterally continuous reflector that tops the acoustic basement is called the ''red event'' [from *Worrall*, 1991]. This reflector marks a major late Eocene boundary between units D and E in the COST well [*Turner et al.*, 1988] (Figure 4), and can be traced throughout the profile (Figure 2). South of transition X, the red event appears to be a disconformity above the horsts and grabens. North of transition X, the horizon becomes an angular unconformity separating the underlying tilted beds of the ''carapace sequence'' of *Worrall* [1991] from the onlapping sedimentary sequence of the BBB. The BBB reflectors above the red event are characterized by high reflectivity, and are subhorizontal, moderately continuous, mostly conformable horizons. The discontinuous reflectors within the grabens beneath the red event are also highly reflective at lower frequency.

[19] It is important to note that on the south margin of the BBB there is no equivalent of the gradual northward thinning (Figure 1). In contrast to the north, about 20 km south of A in Figure 2, other authors have traced the red event upward to the seafloor on the Black Hills ridge [*Marlow et al.*, 1987; *Worrall*, 1991]—a very rapid southward basin thinning. However, because north dipping reflectors downlap onto the unconformities just north of the Black Hills ridge [*Worrall*, 1991], the red event might alternatively be traced from north to south downward beneath the Black

Figure 2. (opposite) Geophysical data compilation. From top to bottom: total intensity magnetic anomaly, free-air gravity anomaly, depth-to-seafloor (all from shipboard data), time-migrated depth-converted seismic reflection data, and structural interpretation. The black vertical line beneath the star (at km 27) marks the location of the COST well. Sonobuoy-derived seismic refraction velocities are given along a diagonal line because the profile is unreversed, and thus successively higher subsequent velocities are from interfaces with greater depth and offset. Tiny squares (at km 20, 27, and 78) indicate the locations used in thickness ratio calculations (Figure 5). Thick black lines represent the basement contact, dashed where uncertain. Thinner black lines are interpreted faults. The white dotted line is the gravity-modeled basement below the proposed carapace sequence (Figure 7). Stratigraphic units have been assigned biostratigraphic dates [*Turner et al.*, 1988]: E - early or middle Eocene to late Eocene, D - late Eocene to middle Oligocene, C - middle Oligocene to late Oligocene, B - late Oligocene to Pliocene, and A - Pliocene to Quaternary. Bold white arrows point at events with southward apparent dips. Transitions X and Y are based on reflectivity and potential field characteristics (see text). Shading represents density (see key for scale) as derived from gravity modeling. [See enlarged version of this figure in the HTML.]

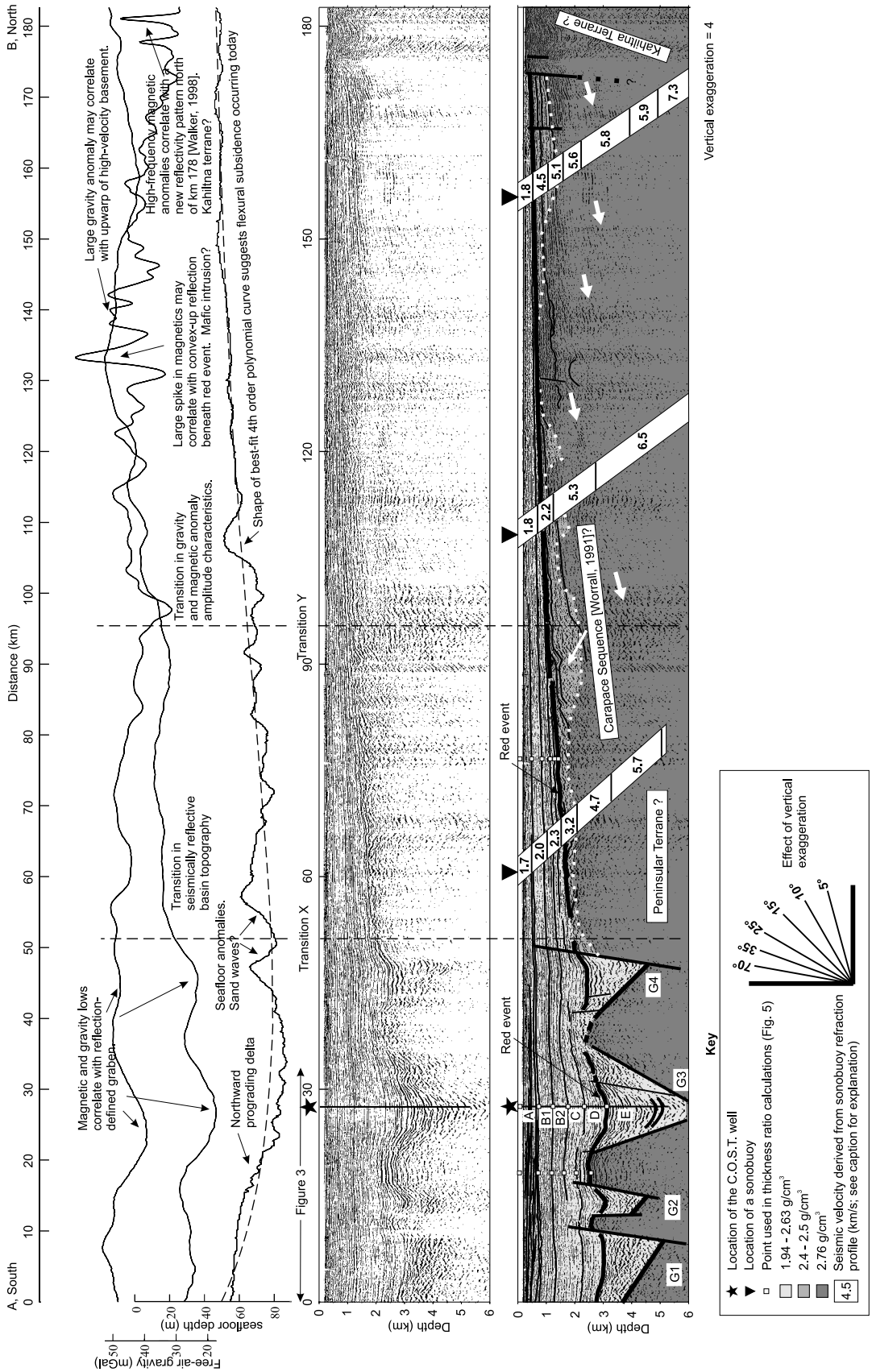
A. South
B. North
Distance (km)
Magnetic anomaly (nT)
Free-air gravity (mGal)
seafloor depth (m)
Depth (km)
Magnetic and gravity lows correlate with reflection-defined graben.
Northward prograding delta
Seafloor anomalies. Sand waves?
Transition in seismically reflective basin topography
Transition in gravity and magnetic anomaly amplitude characteristics.
Large spike in magnetics may correlate with convex-up reflection beneath red event. Mafic intrusion?
Large gravity anomaly may correlate with upwarp of high-velocity basement.
High-frequency magnetic anomalies correlate with a new reflectivity pattern north of km 178 [Walker, 1998]. Kahiltna terrane?
Shape of best-fit 4th order polynomial curve suggests flexural subsidence occurring today
Figure 3
Transition X
Transition Y
Red event
Peninsular Terrane ?
Carapace Sequence [Worrall, 1991]?
Kahiltna Terrane ?
Vertical exaggeration = 4
Key
Location of the C.O.S.T. well
Location of a sonobuoy
Point used in thickness ratio calculations (Fig. 5)
1.94 - 2.63 g/cm3
2.4 - 2.5 g/cm3
2.76 g/cm3
Seismic velocity derived from sonobuoy refraction profile (km/s; see caption for explanation)
Effect of vertical exaggeration

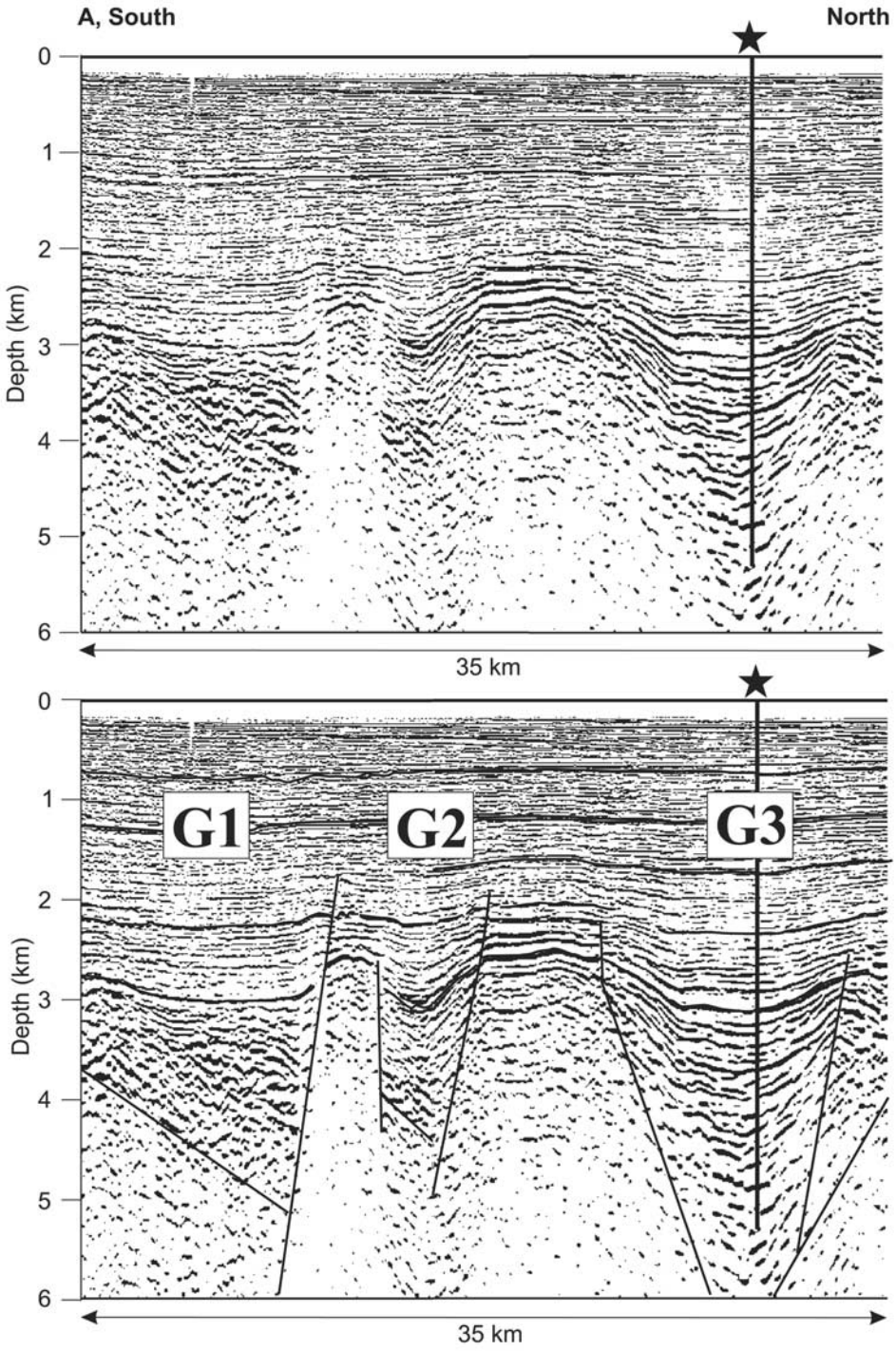

Figure 3. Enlarged section showing faulted basement interpretation south of transition X. Above are the data. Below is the interpretation from south to north: half-graben (G1), small graben (G2), and a large graben (G3). The black vertical line beneath the star is the location of the COST well (Figures 2 and 4). This interpretation is supported by the gravity data and modeling (Figure 7). The 4× vertical exaggeration is the same as in Figure 2.

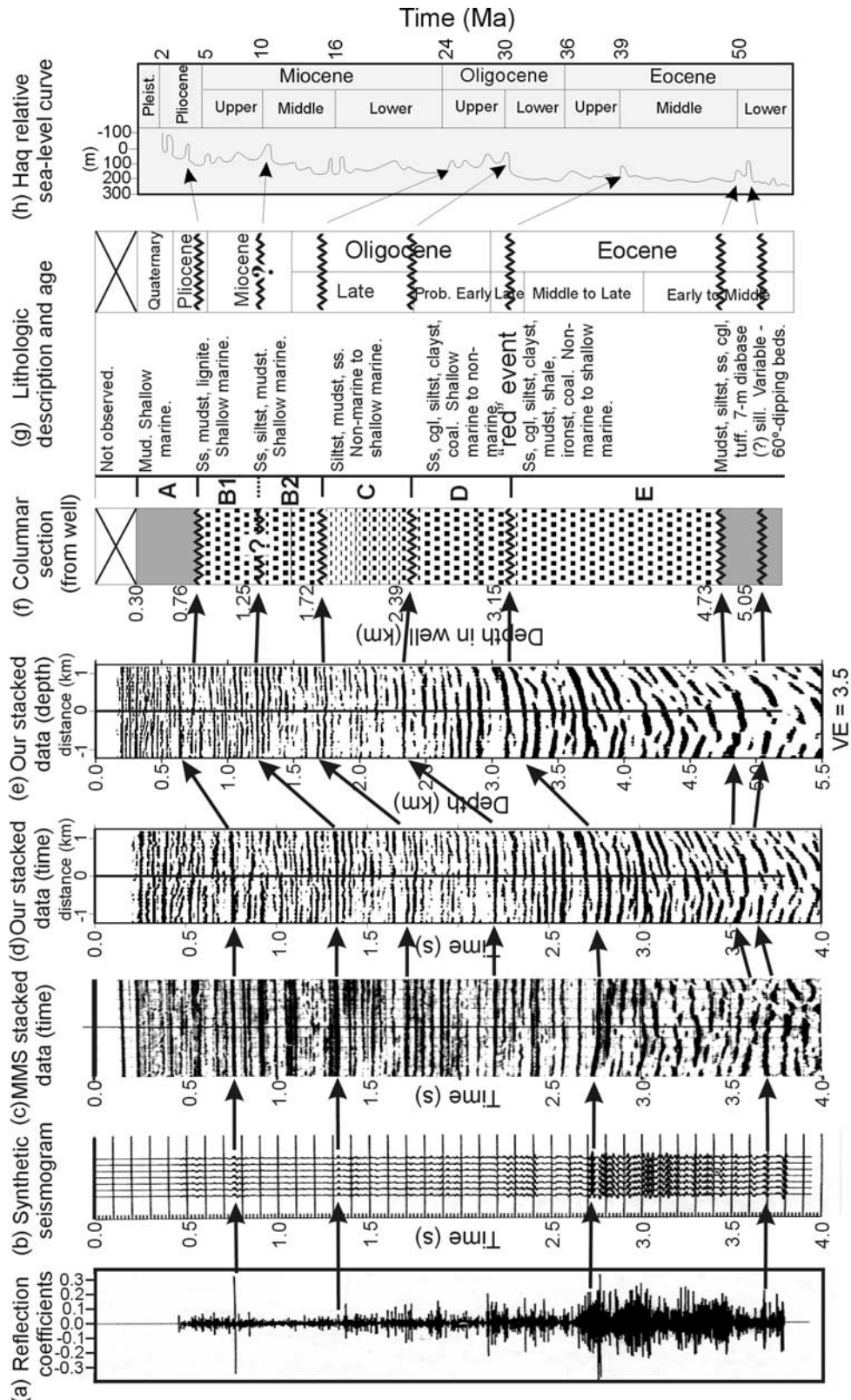

Figure 4. Lithologic correlation diagram: (a) seismic reflection coefficients calculated from the sonic-log velocities from the COST well; (b) synthetic seismogram created from convolving (a) with a standard Ricker wavelet; (c) comparison of the synthetic data with seismic data collected by the Mineral Management Service near the well; (d) our seismic data in the time domain; (e) depth-converted seismic data from (d) with 3.5 vertical exaggeration; (f) lithologic column derived from lithologic data and unconformity depths; (g) the lithologic description and biostratigraphic ages of the units identified in the COST well; and (h) the proposed eustatic sea level curve [*Haq et al.*, 1987]. Data and/or figure in a–c and f–g from *Turner et al.* [1988]. Note the good correlation between the prominent seismic reflectors, unconformities, and periods of eustatic sea level fall.

Hills ridge, indicating no southward basin thinning at all. Consistent with this, *Bond et al.* [1988] points out that data from the COST well, two onshore wells, a sonobuoy refraction line, and multichannel seismic data may suggest that the BBB floor extends beneath the northern coast of the Alaska Peninsula. But in either case, it is clear that the post-red, regional basin subsidence that has occurred is laterally asymmetric and was greatest in the south.

5.2. Basin Reflection Correlation to COST Well

[20] Figure 4 shows the six principal unconformities that have been identified at the COST well in G3 (Figure 2), and their biostratigraphic ages [*Turner et al.*, 1988]. These unconformities correlate well in depth with the seismic reflectors at the COST well, allowing one to carefully extrapolate the lithologic data across the basin. The most remarkable of these unconformities is the late Eocene unconformity. This unconformity correlates with the red event, and has experienced a much longer erosional history north of transition X, as indicated by northward-onlap of late Eocene-Oligocene reflectors in that region. The history of erosion north of transition X prior to the late Eocene is unclear. For the most part, south of transition X, a good correlation exists between the ages of the unconformities and the times of eustatic sea level fall [*Haq et al.*, 1987] (Figures 4g and 4h).

[21] Since most of the prominent seismic reflectors extend throughout the profile, and correlate well with unconformities at the COST well, the stratigraphic column has been divided into seismic sequences as units A, B1, B2, C, D, and E (Figures 2 and 4). Stratigraphic analysis of these units provides a high–resolution record of the basin's subsidence history, and is discussed in the following section.

5.3. Stratigraphic Analysis and Interpretation

5.3.1. Unit E

[22] The COST well penetrated sedimentary sequences of early to middle (?) Eocene to late Eocene age. The depth and age of the graben basement is not known. The red event represents a late Eocene unconformity, and marks the upper boundary of this unit. The sedimentary deposits of unit E are almost completely derived from volcanic source rocks [*Turner et al.*, 1988], probably from erosion of the Peninsular terrane or uplifted carapace fault blocks, and were deposited in a non-marine depositional environment. The early deposition of this non-marine unit was coeval with the final deposition of the non-marine carapace sequence on other parts of the shelf [*Worrall*, 1991] and thus the unit may represent a continuation of carapace sequence deposition while such deposition ceased elsewhere (e.g., north of transition X). Based on the similarity of reflector frequency, amplitude, and continuity within G3 with other grabens, unit E appears to be common to all the grabens.

[23] G1 and G4 appear to be half-grabens overlying rotated fault blocks, with sedimentary reflectors dipping 10–15° northward and truncating against north flanking master faults with apparent dips of ~70° south. Within G4, the reflectors of unit E are discontinuous, suggesting that they have been deformed by minor fault splays off the master fault. In contrast to the dipping reflectors in G1 and G4, the reflectors in G2 and G3 are concave up, suggesting symmetrical subsidence. In all of these grabens, the increasing dip with depth within the half-grabens is interpreted to indicate that deposition was syntectonic, and kept pace with subsidence.

[24] The COST well penetrated a ~7-m thick diabase (?) sill in the lower part of unit E [*Turner et al.*, 1988]. K-Ar dating of this sill yielded a cooling date of 40.5–47.1 Ma. The emplacement of the basaltic intrusion at the COST well is consistent with our interpretation that the BBB experienced rifting.

5.3.2. Units D and C

[25] Above the red event, the late Eocene through early Oligocene interbedded sandstone and shale of unit D and the late Oligocene interbedded sandstone and siltstone in unit C represent the general transition from non-marine to shallow marine depositional environments [*Turner et al.*, 1988]. Both these units were derived from volcanic and metamorphic source rocks.

[26] Unit C is not clearly separable from overlying B2 in some places because the Oligocene unconformity between them exhibits poor reflective continuity to the south, probably a result of bioturbation [*Turner et al.*, 1988]. However, the thicknesses of most units above the red event are laterally variable south of transition X. This lateral variation is interpreted to represent mostly syntectonic deposition. We roughly estimate the amount of fault-controlled subsidence by looking at the ratio of unit thicknesses across the faults. We define this ratio as $R_f = T_g/T_h$, where T_g and T_h are the thicknesses of the units above the grabens and horsts, respectively (Figure 5). When $R_f = 1$, fault-controlled subsidence has ceased. We use the fault on the south side of G3 for this calculation, and the points we use are shown in Figure 2 (tiny squares). We calculate uncertainties based on the frequency content of the reflectors (i.e., the lower the frequency, the more uncertainty in the location of the boundary, and the larger the error). This estimate does not account for compaction, which probably results in two competing biases: (1) overestimation of R_f because of differential compaction of underlying units, and (2) underestimation of R_f because of differential compaction of the unit being analyzed.

[27] Many of the seismically interpreted horst and graben faults penetrate through unit D and die out in unit C. The thickness of unit D across the south flanking fault of G3 varies significantly from 510 m above the horst to 790 m in the graben, yielding an $R_f = 1.5 \pm \frac{0.2}{0.2}$. The thickness of unit C is 450 m overlying the horst and 600 m thick in G3, producing an R_f of $1.3 \pm \frac{0.1}{0.1}$. These data suggest that fault-controlled subsidence was probably active but waning from late Eocene to late Oligocene.

[28] Reflectors in units D and C can be traced north until they onlap the red event as far north as km 110. Given the first-order sea level regression interpreted at this time as in the *Haq et al.* [1987] sea level curve, this onlap implies regional subsidence occurred at least from the late Eocene

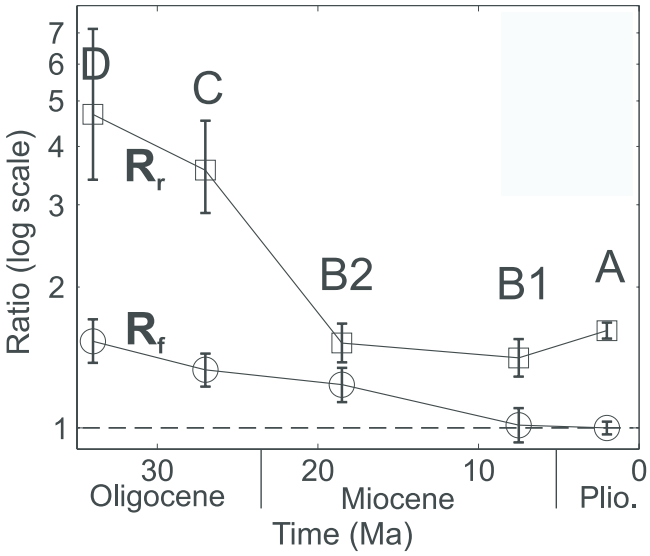

Figure 5. Pseudo-subsidence curves for different mechanisms estimated from unit thickness ratios as a function of time. Circles represent fault-controlled subsidence (R_f); squares indicate regional subsidence (R_r). Locations used are shown in Figure 2. Times for these data points come from the middle of the time range over which the unit was deposited. Measurement error varies because of the lateral and vertical variation of reflector frequency content, and is amplified in R_r (Oligocene) because the thickness in the denominator is very small.

and continued through the Oligocene. To quantify the relative amounts of regional subsidence, we define a ratio $R_r = T_s/T_n$, where T_s and T_n are southern and northern unit thicknesses. The northern thicknesses are calculated at km 78, but the southern thicknesses are calculated by averaging the thicknesses and errors associated with the horst and graben calculations (km 19 and km 28; Figure 2). Again, compaction is not accounted for in this estimate, but this could only lead to underestimates of R_r (due to differential compaction of the unit being analyzed) because differential compaction of underlying units would have been averaged out because of the relative uplift and subsidence associated with local basement faulting in the south.

[29] Unit D thins from 650 m in the south to 140 m at km 78, yielding $R_r = 4.6 \pm {}^{2.4}_{1.3}$. Similarly, unit C thins from 530 m to 150 m, so $R_r = 3.5 \pm {}^{1.0}_{0.7}$. Thus regional subsidence was strong in the late Eocene, but was probably waning by the late Oligocene (Figure 5).

5.3.3. Unit B

[30] Unit B consists of a thick sedimentary sequence of late Oligocene, Miocene, and early Pliocene age. The provenance and depositional environments are similar to those in units C and D. A prominent high-amplitude reflector separates the unit into upper and lower subunits B1 and B2, respectively. This basin-wide reflector correlates well with a lithologic boundary, separating diatom-rich sediment above from diatom-poor sediment below [*Turner et al.*, 1988]. It may also represent a middle to late Miocene unconformity, as suggested by the large eustatic sea level drop during that time period [*Haq et al.*, 1987].

[31] The thickness of unit B2 varies only slightly from 410 m over the horst to 510 m in the graben (Figure 2). This leads to an R_f of $1.2 \pm {}^{0.1}_{0.1}$, not much less than the 1.3 estimate for the underlying unit C (Figure 5). The 500-m thickness of the overlying unit B1 is constant over the horsts and grabens (R_f = 1.0). These data suggest that fault-controlled subsidence waned in the Oligocene and ceased around the middle Miocene. However, the normal fault at transition X offsets strata as young as early Pliocene.

[32] In general, the thicknesses of units B1 and B2 are laterally constant over several tens of kilometers south of transition X. However, these units consistently thin to the north into a veneer of sediment that drapes the red event. Unit B2 thins from 460 m to 300 m ($R_r = 1.5 \pm {}^{0.2}_{0.1}$) at km 78 where its reflectors begin to onlap underlying unconformities. Unit B1 thins from 490 m to 350 m, leading to an $R_r = 1.4 \pm {}^{0.1}_{0.1}$ (Figure 5). Compared with the larger R_r for the underlying units, these ratios and the onlapping relationships observed in the data strongly suggest that regional subsidence continued but waned during the Oligocene-Miocene.

5.3.4. Unit A

[33] Unit A is comprised of unconsolidated volcaniclastic sediments of late Pliocene to Quaternary age [*Turner et al.*, 1988]. In general, these sediments downlap to the north between km 0 and km 50 (Figure 2). In some locations, these surfaces appear to be angular unconformities as they appear to truncate underlying reflectors.

[34] The reflectors in unit A define three sequences of clinoforms. *Turner et al.* [1988] reported that such clinoforms occur throughout the BBB, and interpreted them as part of a northward prograding delta system, probably originating from the erosion of volcanic centers on the Alaska Peninsula. This interpretation is further supported by the fact that the age and lithology of this section is similar to that of the Pliocene Milky River Formation on the Alaska Peninsula *Brockway et al.*, 1975].

[35] Using the depth to the seafloor as the upper boundary, unit A gradually thins from 660 m in the south to 410 m at km 78 (Figure 2), yielding an $R_r = 1.6 \pm {}^{0.1}_{0.1}$ (Figure 5). Although within the uncertainty, this value is larger than that for unit B1, and the rate of regional subsidence possibly increased from the Miocene through the Holocene.

5.3.5. Summary of Stratigraphic Analysis and Interpretation

[36] The late Eocene unconformity at the COST well correlates with a strong seismic reflector. This reflector extends throughout the entire profile, and has been mapped as the "red event" [*Worrall*, 1991]. South of transition X, the horizon is locally concordant with overlying basin fill. North of transition X, it is onlapped by Oligocene and Miocene basin fill, suggesting the red event is time-transgressive and reflects a much longer non-depositional history in the north. Throughout the profile, the red event appears to separate primarily non-marine sedimentary units below from shallow-marine units above. North of transition X, these non-marine units comprise the carapace sequence.

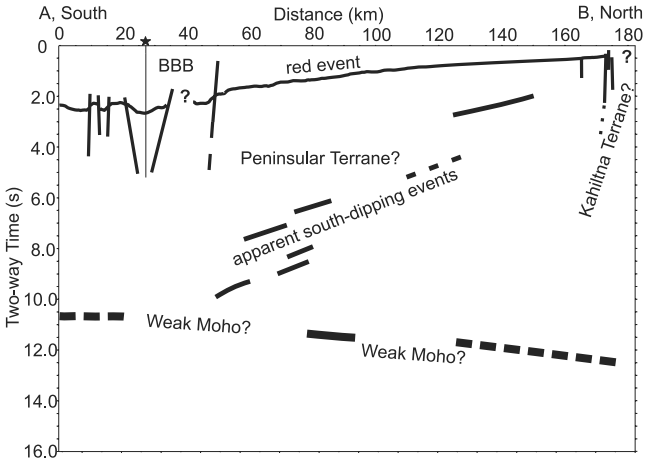

Figure 6. Deep reflection line drawing. It appears that the Moho is only very weakly reflective throughout the profile. It can be identified between km 80–95, but coherent noise makes it difficult to distinguish north of km 100. The apparent south dipping events may be reflectors or coherent noise.

South of transition X, these non-marine units are probably younger and comprise the Eocene depositional units of the BBB.

[37] The geometry of shallow reflectors in our profile, and their stratigraphic relationships with the red event, strongly suggests that two different mechanisms contributed to Bristol Bay basin subsidence. The thickness ratios suggest that fault-controlled subsidence ceased in the middle Miocene. However, a large normal fault at km 50 clearly extends upward into the upper strata of unit B1. Thus the fault-controlled subsidence phase, which produced grabens and half-grabens in the pre-basin surface, began by the middle Eocene or earlier, and continued throughout the late Miocene. An asymmetric regional subsidence phase, largest in the south, began in the late Eocene, and continued to the present day. This regional subsidence phase was initially rapid, began to wane by at least the late Oligocene-Miocene, then possibly increased again from the late Miocene-Holocene during a period of renewed volcanic activity on the Alaska Peninsula that supplied sediment for a northward prograding delta system.

5.4. Deep Seismic Data

[38] The deep-data processing was very similar to that of the shallow data, but because we focused on removing coherent noise that was prominent at far-offsets on CMP gathers between 6–16 s TWT (as opposed to removing multiples on the shallow data), we did not use a far-offset-weighted stacking function. Because our overriding concern was to preserve the shallowly (<15°) dipping events, this processing attenuated only some, and not all, of the coherent noise in the deep data.

[39] Unfortunately, the deep data do not show much detail. Figure 6 shows a line drawing of the events identified in the deep data. For displays of the actual CMP-stacked data, see *Walker* [1998]. The most important observations are the lack of mid-crustal reflectivity and a poorly defined, weakly reflective Moho. In addition, it appears that a weak south dipping reflection fabric exists from km 60 to km 170. However, the poor signal-to-noise ratio permits the possibility that these south dipping events are residual multiple energy or coherent noise.

6. Sonobuoy Refraction Data

[40] Sonobuoys were also deployed along the profile to collect refraction data out to ~30-km offset (Figure 1). J. Diebold (Columbia University, unpublished data, 1997) calculated 1-D velocity models based on these data to a maximum depth of 7 km (Figure 2), assuming that all interfaces were horizontal, that the velocities of successive layers increased with depth, and that a linear velocity gradient existed in each layer. We used the average velocity of each layer to create 1-D velocity profiles with which to compare reflection data and gravity modeling results. Some interfaces separating thin units of similar velocity are not indicated. Since the seismic vessel acquired data while moving from south to north, the 1-D velocity models sample the velocity structure along a diagonal line that dips north (Figure 2).

[41] In general, the seismic velocities increase toward the north for any given depth, with the greatest increase between km 70 and km 120 suggesting a basement uplift around km 120 (Figure 2). This interpretation is also consistent with the apparent south dipping seismic reflectors beneath the red event. Figure 2 also shows a fair correlation between velocity interfaces and reflectors, suggesting the red event is a lithologic boundary between Late Cenozoic sedimentary units above, and probably either Late Cretaceous-middle Eocene sedimentary units (carapace sequence?) or crystalline units (Peninsular Terrane?) below.

7. Gravity Data

[42] We collected high-quality gravity data along the reflection profile (Figure 2), logging data every second with a Bell Aerospace BGM-3 marine gravimeter. The Data Reduction Group at Lamont Doherty Earth Observatory reduced the raw data (B. Arko, Columbia University, personal communication, 1998) by passing them through a 60-point Gaussian filter and resampling every 60 s (~120 m).

7.1. Description and Interpretation

[43] The shape of the free-air gravity anomalies are, in general, characterized by 5-to-10-km long undulations superimposed on a regional anomaly of +0.17 mGal/km (~30 mGal increase from A to B) (Figure 2). The anomalies south of transition X mimic the shape of the interpreted basement topography, as prominent gravity highs (~28–29 mGal) occur over the horsts and prominent lows (~18–25 mGal) occur over the grabens. On the basis of changes in potential field anomaly characteristics, we introduce transition Y at km 96. Between transitions X and Y, the data contain undulations of ~3 mGal superimposed on a broader

high of ~35 mGal. The undulation at km 66 may reflect the presence of a syncline beneath the red event, since the red event truncates apparent north dipping strata between km 50–66 and south dipping strata between km 66 and transition Y. The anomalies north of transition Y appear to vary rapidly from 32 to 52 mGal, probably a result of topography along a non-reflective basement contact underlying the red event and/or subsurface density anomalies associated with plutonic bodies.

[44] The 30-mGal regional anomaly suggests that isostasy is not maintained along the profile. Over such a long distance (~180 km), such a situation could arise if a dynamic stress is currently loading the southern portion of the BBB. *Bond et al.* [1988] previously noted this pattern, and interpreted it to be due to deflection of the lithosphere from crustal loading on the Alaska Peninsula. This is also consistent with the seafloor depth profile (minus the shallow depth in the south due to a northward prograding delta; Figure 2), which shows a deflection that is predicted well by a 4th-order polynomial (i.e., a solution to the flexure equation).

7.2. Modeling and Interpretation

[45] To better constrain our structural interpretation beneath the stratigraphy sampled by the COST well, we forward-modeled the gravity data using constraints provided by the interpreted seismic reflection and well-log data. The seismic data provided the geometry of the density contrast interfaces, and the well-log data provided the densities at the top and bottom of each layer. We then vertically interpolated and laterally extrapolated the density function through each layer, while simulating the effects of compaction by roughly maintaining a constant density at depth within each layer despite undulations in the layer interfaces.

[46] Three density models were developed to account for the observed data. Once the intralayer density extrapolation was completed, we held these intrabasin densities fixed, and varied the basement density, dip of graben-bounding faults, and Moho topography to arrive at Model 1 (Figure 7). This model has a 2.76 g/cm^3 basement that is faulted by low- to high-angle normal faults, overlying a north dipping Moho from a 33-km depth at the south end to 40-km depth at the north end. This Moho topography is generally consistent with the depth of our reflection Moho interpretation (Figure 6), surface-wave studies [*Niazi and Chun*, 1989] and other Moho depths found as part of the Pacific to Bering Shelf Deep Seismic Experiment [*Fliedner and Klemperer*, 1999, 2000; *Lizarralde et al.*, 2002]. Note that the Moho dips a little more steeply to the south of transition X (beneath the faulted part of the BBB) than from transition X to km 180, consistent with extension having caused crustal thinning beneath the BBB.

[47] For Model 1, the calculated data agree well with the observed data south of transition X, supporting the horst and graben interpretation for the basement topography. The Peninsular terrane has been interpreted to underlie the carapace sequence throughout the outer and southern Bering Shelf [*Worrall*, 1991; *Klemperer et al.*, 2002]. Because the graben at the COST well contains volcaniclastic strata probably derived from the uplifted footwalls, the 2.76 g/cm^3 horsts beneath the southern part of the basin are probably comprised of volcanic rocks of the Peninsular terrane [*Jones and Silberling*, 1979].

[48] One interesting feature of the model is that the modeled gravity lags the observed gravity (e.g., the top of the horst between G2 and G3 is at km 20, but the corresponding gravity high is at km 17; Figure 7). This lag cannot be removed by varying the dip of the fault planes, and is consistent to some degree over most of the horst and graben topography. This lag can be explained by a violation of the assumption of 2D structure in the gravity modeling, in particular, if the grabens, which on average strike WSW-ENE [*Worrall*, 1991] and about 65° from the N-S profile, bend a little toward the south on the west side of the profile.

[49] Model 1 implicitly assumes that the red event north of transition X is the top of crystalline basement, and that no significant lateral density variations exist below that surface, as suggested by the weak seismic reflectivity in this region. Clearly, the calculated data for this model do not fit the details of the observed data north of transition X, and the crust beneath the red event is more heterogeneous than predicted by the reflection data. This point is supported by the refraction velocity data, which indicate strong lateral and vertical seismic velocity variability.

[50] One approach to fitting the observed data north of transition X is through the modeling of simple, polygonal bodies with anomalous densities. Thus for Model 2, we held fixed the best fit parameters from Model 1, while varying the density contrast and geometry of two introduced crustal masses (Figure 7). The best fit densities for these masses were 2.5 g/cm^3 and 3.0 g/cm^3. This model of adjacent felsic and mafic plutons has no supporting evidence. Rather, the purpose of Model 2 is to show the scale and magnitude of the density anomalies that would be required to fit the undulations north of transition X.

[51] Our preferred approach to fitting the data north of transition X is to assume that the weakly reflective basement is the broadly deformed carapace sequence of *Worrall* [1991]. Assuming an average density contrast of ~0.3 g/cm^3 between the carapace and the underlying basement, we created a carapace model (Model 3) where we removed the anomalous crustal masses of Model 2 and instead added another interface beneath the red event, and varied the geometry of this interface to fit the observed gravity undulations not fit by Model 1. We believe the first-order features in Model 3 north of transition X represent topography along the contact between the carapace and the Peninsular terrane (Figure 7). The contact's shape roughly correlates with patterns of reflectivity, and the contact's location correlates well with large increases in the refraction velocities at km 70 and km 112 (Figure 2). The rapid jumps in topography between km 100 and km 125 may suggest the presence of faults.

8. Magnetic Data

[52] Magnetic data were collected synchronously with the gravity data using a Varian V75 magnetometer. Initially

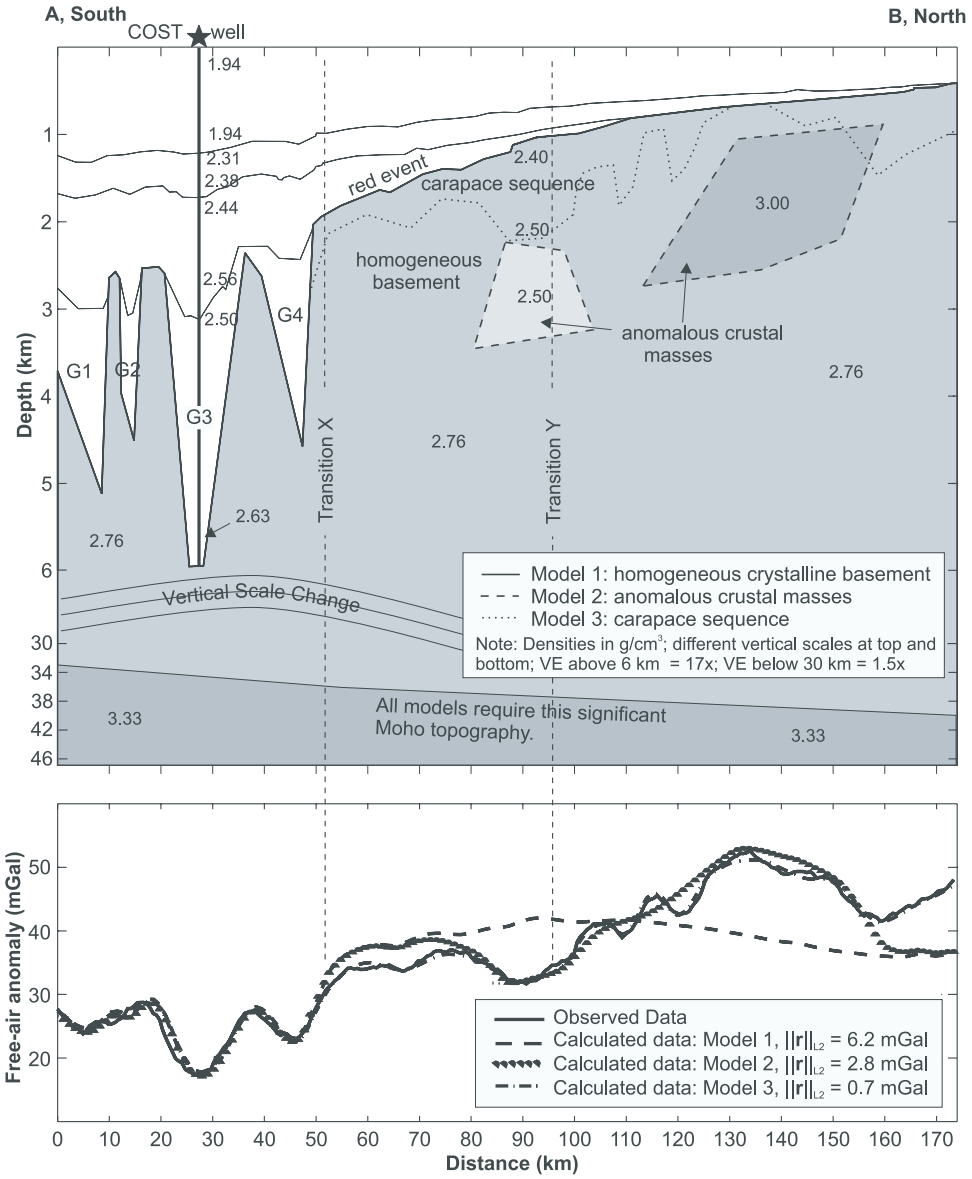

Figure 7. Gravity modeling results. (a) Structure model for three different gravity models: homogeneous basement, anomalous crustal mass, and carapace basement model. (b) Calculated free-air gravity and its comparison to the observed gravity. The carapace basement model (Model 3) is the preferred model, and it is supported by the refraction velocity data, magnetic data, and to an extent, the reflection data (Figure 2).

collected every 6 s, these data were passed through a 10-point exponential filter and resampled every 60 s (~120 m).

[53] The magnetic anomalies south of transition X, and to some extent north to transition Y, correlate fairly well with the gravity anomalies (Figure 2). However, because magnetic anomalies arise from a dipolar source, and the Earth's magnetic field has an average inclination of 70° along the profile, the magnetic anomalies from deeper sources are displaced to the south. This displacement is evident from the broad 300-nT low between km 15 and km 35, which is probably due to a magnetization contrast between the sediments and flanking basement in G3. The broad, low-amplitude anomalies are characteristic of sedimentary basins, and further support the interpretation of the carapace sedimentary sequence beneath the red event north of transition X (at least to transition Y).

[54] North of transition Y, undulations in the magnetic data increase in frequency. These undulations are especially high in frequency where broad gravity highs exist (i.e., km 125–150; km 175–182), suggesting that the anomalies are due to magnetization contrasts in shallow high-density basement. These observations are consistent with the apparent south dipping reflectors beneath the red event and the apparent increase in seismic velocity toward the north for any given depth. Together, these data suggest that

the basement shallows toward the north, most dramatically from km 80 to km 130. In addition, a convex-up reflector, located almost directly beneath the km-133 anomaly, may suggest a correlation with a plutonic body or inactive subsurface fault. These magnetic observations are similar to those discussed by *Worrall* [1991], who interpreted the back arc region in the Late Cretaceous as being eroding highlands with scattered magmatism.

9. Flexural Modeling and Interpretation

[55] One of the most obvious features of the BBB is the lateral asymmetry of regional subsidence; the BBB is deepest in the south, and gradually thins to the north. This gradual shoaling of the basement appears to be nonlinear with increasing distance to the north, and is reminiscent of that produced by deflection of a loaded elastic plate.

[56] Such a hypothesis, assuming a volcanic load, was first proposed and tested by *Bond et al.* [1988]. These workers used an assumed basement seismic velocity of 6.0 km/s to derive four depth-to-basement points from sonobuoy refraction data (C–D; Figure 1), and then projected these points onto a transect orthogonal to the volcanic arc (C′–D′). They used these projected points in an elastic cantilever-beam model loaded at its broken end by a volcanic load [*Jordan*, 1981; *Karner and Watts*, 1983], and used gravity modeling to constrain the size and lateral position of their load beneath the Alaska Peninsula. Bond et al. concluded that their model was not consistent with the hypothesis of volcanic loading of the arc because their model demanded an unrealistically high load elevation. They further stated that the load could not be plutonic, because that would require an unrealistic load density.

[57] Since the seismic reflection data presented in this paper allow us to define a better paleosurface (the red event) with which to compare deflection models, we return to the initial hypothesis of *Bond et al.* [1988] that post late Eocene regional subsidence was due primarily to flexure of the lithosphere from volcanic loading of the plate. Lithospheric flexure has been successfully used to explain subsidence of mid-plate volcanoes [*Walcott*, 1970; *Watts and Cochran*, 1974; *Watts*, 1978], oceanic-plate warping seaward of subduction zones [*Hanks*, 1971; *Watts and Talwani*, 1974], and deformation in other active tectonic regions [*Lyon-Caen and Molnar*, 1983; *Sheffels and McNutt*, 1986; *Jin et al.*, 1996]. We tested three different models of deflection of the seismically defined red event (Late Eocene unconformity) in response to an ''apparent'' load using a two-dimensional finite-difference modeling algorithm similar to that of *Sheffels and McNutt* [1986], but with different boundary conditions.

[58] Seismic tomographic imaging [*Fliedner and Klemperer*, 1999; *Lizarralde et al.*, 2002] shows a 40-km wide high-velocity body at 5–8 km depth in the crust of the Aleutian forearc region. We further constrained the lateral position of this assumed high-density body using the tomography beneath eastern Unimak Island [*Fliedner and Klemperer*, 2000], and then extrapolated it to the forearc/arc edge of the Alaska Peninsula using gravity data [*Barnes et al.*, 1994]. We interpret the location of the high-density body in the forearc to be the previous location of the arc, and thus for our modeling, we assume an ''apparent'' volcanic load that spans this 40-km wide body and the 50-km wide current arc (Figure 1).

[59] We then took many well-constrained points along the red event (A–B), and projected them onto a nearby transect (A′–B′) that is orthogonal to the apparent load. Points from the red event south of transition X show more scatter in depth because the reflector has been disrupted by fault-controlled subsidence.

[60] For all three models, the density of the apparent load was set at 2.9 g/cm^3, because arc volcanism had a basaltic to dacitic composition [*Moll-Stalcup*, 1994]. The density of the basin fill was set at 2.25 g/cm^3, the average density of the sediments overlying the late Eocene unconformity at the COST well, and the mantle density was fixed at a standard 3.3 g/cm^3. Young's modulus was fixed at 10^{11} N/m^2, approximately that of diabase [*Burger*, 1992], and Poisson's Ratio was fixed at 0.25.

[61] In our modeling, the height of the apparent volcanic load above the flexed plate (h) and the apparent elastic thickness of the plate (T_e) were free variables. We term the free parameters as ''apparent'' parameters because the deflection problem can be represented in many different ways and can include or preclude many different unknown factors. For example, in a ''continuous'' lithosphere model where h = 10 km and T_e = 15 km, the deflection directly beneath the load is 6 km. However, for a lithosphere model ''broken at the load center,'' to get the same deflection of 6 km with the same load requires T_e = 45 km. This would be a huge difference if a physical meaning was attached to T_e, and hence we call T_e ''apparent elastic thickness''. Similarly, if h is unrealistically large for a given model, there are probably additional factors not included in that model that add to the effects of the volcanic load (e.g., tectonic compression, laterally variable elastic thickness and thermal histories, additional loading mechanisms).

[62] Model 1 assumes a continuous lithosphere, extending to infinity in both directions (at least 3 flexural wavelengths), and loaded at the center by the apparent load. The best fit model reproduces the observed data fairly well (Figure 8), with T_e = 42 km and h = 10 km (Figure 8).

[63] For Model 2, we tried a model similar to that used by *Bond et al.* [1988] and assumed the lithosphere was broken at the center of the volcanic arc. The best fit model parameters are T_e = 67 km and h = 11 km. The calculated data from this model fit the observed data no better than that from Model 1.

[64] In addition, we tried a third model similar to that used by *Sheffels and McNutt* [1986] to explain the flexure beneath the San Jacinto Mountains. This model is presumably more realistic than our previous ones because it assumes a lithosphere loaded in the middle, and fixed at the subduction end to have a bending moment M (due to the traction with the subducting plate). The best fit parameters are T_e = 33 km, h = 8.5 km, and $M = 4 \times 10^{10}$ N. Although fitting the observed data slightly better, the improved fit of this model comes at the ends of the profile where significant

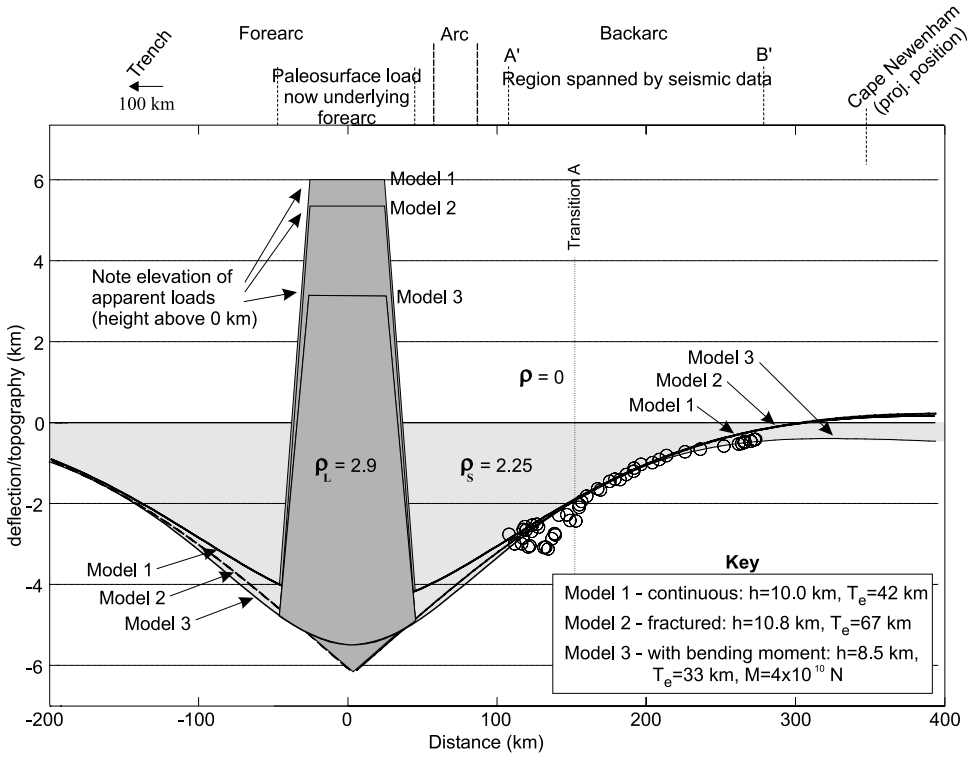

Figure 8. Flexural modeling results. Depths to the red event (circles) were taken from line A–B and projected to A′–B′, a line orthogonal to the apparent load (Figure 1). The key shows the free parameters used in the modeling. All three models produce deflection that fit the data well. Note that Models 1 and 2 predict that Cape Newenham is the flexural bulge associated with back arc flexure.

faulting has occurred (Figure 2), and thus may not be significant.

[65] For these three models, we find that the best fit T_e varies widely (33–67 km), as might be predicted by the different model assumptions used. Although h is rather similar (8.5–11 km) for these models, the magnitude of h is consistently unrealistic. If the actual load on the lithosphere was volcanic, the current load elevations should be 3–6 km (Figure 8). However, the highest elevation in the arc is only 1 km, and this load is about 50 km north of our assumed apparent load. *Bond et al.* [1988] also encountered a similar inconsistency in their volcanic model (they found T_e = 15 km and h = 10 km).

[66] A different way to look at the observed load/deflection inconsistency is to calculate the amount of deflection due to volcanic loading that yields the final current 1-km elevation of the volcanic edifice. We do this for the continuous plate model assuming the same material properties, T_e, and load geometry as above. We find that an initial volcanic edifice elevation of 2 km will produce 1 km of deflection of the arc (leading to the observed 1-km high volcanic edifice of the current arc), and will accommodate only 300 m of sediment fill in the back arc. Since there is actually 3000 m of sediment represented in the seismic data, the discrepancy is huge.

[67] Both our interpretation and that of *Bond et al.* [1988] must explain why the height of the apparent volcanic load is so high (or the predicted deflection associated with current topography so low). To this end, Bond et al. assumed the volcanic model was insufficient by itself, and that BBB deflection was due to crustal thickening along the arc. We propose that volcanic loading was the principal mechanism, but that there were additional factors that contributed to the modeled flexure. The first factor is the additional loading from the lithospheric cooling that followed Eocene extension. From our crustal thickness estimates from refraction and gravity data (Figure 7), the lithosphere experienced about 20% extension. For a simple model of symmetric lithospheric thinning [*McKenzie*, 1978], thermal subsidence associated with 20% extension would accommodate about 700 m of sediment in the deepest part of the basin. This suggests that thermal subsidence explains a significant part of the total regional subsidence, which is represented by 3000 m of sedimentary strata (Figure 2).

[68] Another factor that could have amplified regional subsidence in the back arc is compression associated with the convergence between the North American and Pacific plates [*Cloetingh et al.*, 1989]. Evidence for compression throughout the arc comes from observations of latest Miocene through Pliocene reverse faulting and folding, with beds dipping up to 40° [*Burk*, 1965; *Detterman et al.*, 1981]. Further evidence comes from Miocene high-angle faulting and tight folding with beds dipping up to 80° along the southern coast of the peninsula [*Burk*, 1965;

Wilson et al., 1983]. Finally, the World Stress Map shows maximum horizontal compressive stress orientations in the forearc that are perpendicular to the arc (see "The 2000 release of the World Stress Map," by B. Mueller, J. Reinecker, O. Heidbach, and K. Fuchs, available at http://www-wsm.physik.uni-karlsruhe.de/). If such stresses have been consistent throughout the Cenozoic, then this compression could have amplified back arc deflection.

[69] A third factor that could have contributed to regional subsidence is the additional loading from crustal thickening of the Alaska Peninsula via reverse faulting [*Bond et al.*, 1988] or thrust faulting. Because the observed gravity anomaly associated with the mass we used in our modeling is large, we interpret the load as igneous in origin. However, a complementary possibility is that loading due to reverse or thrust faulting causes some of the regional subsidence. If such loading occurs along multiple faults, then the lithosphere is loaded significantly even if the density contrast across each fault is not great. Hence the gravity and seismic-velocity anomalies associated with a specific thrust-load would be much smaller than for a volcanic load (and so we could not identify them in the tomography and gravity data when we were defining the model load).

[70] A final factor that could have contributed to regional subsidence is the additional loading associated with many small-scale intrusions of dense basaltic magma into less-dense felsic upper crust [*Bond et al.*, 1988]. Our model of a single volcanic load was based on large-scale velocity and gravity anomalies. However, small-scale anomalies were not identified. Smaller-scale loads, however, below the resolution of regional tomographic inversions and gravity surveys, also exist, as shown by the 7-m thick basaltic sill penetrated by the COST well, and have not been specifically modeled.

10. Tectonic Synthesis

[71] Our results, combined with published information about the tectonic history of the region, allow us to interpret the evolution of the Bristol Bay basin. During the Cretaceous, the Peninsular terrane accreted to the continental backstop of the North American plate [*Jones and Silberling*, 1979], deforming the intervening flysch basin of the Kahiltna terrane [*Decker et al.*, 1994]. The Peninsular terrane probably comprises the basement beneath the BBB because it comprises the basement along the northern coast of the Alaska Peninsula, and our gravity data modeling requires a basement density of 2.76 g/cm^3 immediately below the Eocene grabens, an appropriate density for the rocks of the Peninsular terrane. The Peninsular terrane may in fact extend north to km 175, where the beginning of highly deformed basement reflectors may represent the deformed flysch of the Kahiltna terrane [*Walker*, 1998] (Figures 1 and 2).

[72] A hiatus in forearc deposition followed the accretion of the Peninsular terrane, but ended with the Late Cretaceous to middle Eocene deposition of continental to marine shelf units [*Burk*, 1965]. These units probably correlate with the carapace sequence identified on seismic reflection profiles across the Bering shelf [*Worrall*, 1991; *Klemperer et al.*, 2002], and included in our seismic reflection interpretation (Figure 2). Our carapace sequence identification is based on (1) the onlap of basin sediments onto the red event north of transition X (Figure 2), a relationship interpreted to top the carapace sequence throughout most of the region [*Worrall*, 1991; *Klemperer et al.*, 2002], (2) gravity modeling, and (3) correlation between regions of high-frequency magnetic data, high seismic velocity, and broad gravity highs suggesting varying basement topography of a non-reflective basin beneath the red event (Figures 2 and 7).

[73] Recent demonstrations of the lack of fixity of Pacific-plate hot spots [*Raymond et al.*, 2000; *Steinberger and O'Connell*, 2000] will require significant revisions of the previously accepted history of northeast Pacific plate motions [e.g., *Engebretson et al.*, 1985], so any attempt to explain back arc dynamics with published Pacific plate histories is now inappropriate. However, the oldest volcanic rocks in the Aleutian arc are 50 Ma, suggesting that subduction jumped from the outer Bering Shelf margin and initiated beneath the present day arc in the early Eocene [*Marlow et al.*, 1973; *Scholl et al.*, 1987]. In addition, a 60–43 Ma heating event is known to have occurred in the forearc of southeastern Alaska, resulting in high-temperature/low pressure metamorphism, quartz veining, and intrusion of felsic plutons from partial melting of the accretionary prism sediments [*Liou et al.*, 1985; *Plafker et al.*, 1985]. *James et al.* [1989] argued that the heating event may represent the subduction of the Kula-Farallon spreading ridge, or the underplating of young, hot oceanic lithosphere of the Kula plate. However, because of the recognized ambiguity associated with the location of the Kula/Farallon and Kula/Pacific spreading ridges at this time, others have suggested that one or both of the Kula ridges stopped spreading before entering the trench [*Jackson et al.*, 1978; *Byrne*, 1979], and/or was subducted beneath the Aleutian Islands later in the Oligocene [*DeLong and Fox*, 1977].

[74] *Worrall* [1991] suggested that the ~43-Ma northward to north-northwestward change in plate convergence direction, which was found assuming fixed Pacific hot spots, caused a right-lateral strike-slip fault zone to develop along the outer Bering shelf and southwest Alaska Peninsula. Specifically, he argues that the outer shelf basins and the BBB are all associated with strike-slip deformation via (1) folding immediately prior to 43 Ma, (2) uplift and right-lateral strike-slip faulting at 43 Ma, and (3) continued but waning strike-slip-faulting through the Miocene. He argues that the BBB is the northern conjugate of the Black Hills ridge, i.e., basin subsidence occurred by strike-slip related extension contemporaneously with the uplift of the Black Hills.

[75] The N65°E trending structures that *Worrall* [1991] interprets as folds we interpret as horsts and grabens based on our seismic reflection interpretation and gravity modeling (Figures 2, 3, and 7). The precise timing of the onset of fault-controlled subsidence in the Bristol Bay basin is not known. However, this subsidence was clearly occurring during early-to-middle Eocene time (Figure 4), contemporaneously with the heating event in the forearc and initiation

of subduction beneath the Aleutian islands. For the BBB faults identified on line A-B, fault-controlled subsidence generally ceased by the middle Miocene as suggested by the nearly uniform thickness of unit B1 above the horsts and grabens (R_f, Figure 5). However, the termination of the large normal fault in the top of unit B1 at km 50 (Figure 2) suggests faulting did not completely cease until the early Pliocene.

[76] In the gravity modeling (Figure 7), the modeled gravity lags the observed gravity in the southern portion of the profile (compare observed high at km 18 with modeled high at km 20). If the horst-and-graben structures, which were seismically imaged directly beneath the profile and strike WSW-ENE on average, bend toward the south on the west side of the N-S profile, this would explain the phase lag between the calculated and observed gravity as a violation of the 2D assumption used in our gravity modeling.

[77] We suggest that fault-controlled subsidence and the emplacement of igneous rocks in the COST well were due to about 20% extension in the Bristol Bay region, as suggested by the thinning of the crust (33-km Moho at south end, 40-km thick Moho at north end; Figures 6 and 7). This minor extension is also consistent with the lack of a reflective Moho and mid-crustal reflectivity (Figure 6), two common attributes of highly extended regions.

[78] Recent plate reconstructions incorporating hot spot wander [e.g., *Raymond et al.*, 2000] remove, reduce, or change the previously accepted 43-Ma change in plate convergence [e.g., *Engebretson et al.*, 1985], and cast doubt on the accuracy of *Worrall*'s [1991] assumed 43-Ma onset of strike-slip faulting. Our preferred model is similar to that proposed by Worrall, except that we suggest the strike-slip faulting along the borders of the Black Hills ridge and associated basement normal faulting in the back arc to have begun earlier, at the latest by early-to-mid Eocene (55–45 Ma). In such a right-lateral system, one would kinematically expect localized stress complications (both compressive and tensile) and fault-controlled subsidence in the proximity of the bend of the strike-slip faults that border the Black Hills ridge (Figure 1). The driving forces for this strike-slip faulting and associated stresses are unclear, but we speculate that because strike-slip faulting appears to have been continuous throughout most of the Tertiary and not just associated with one particular event, the most probable candidates are forces associated with escape tectonics from mainland Alaska, i.e., westward push from southern mainland Alaska to create room for northward verging terranes in the Coastal Mountains of western British Columbia and southeastern Alaska (T. F. Redfield et al., Plate kinematics and escape tectonics in Cenozoic Alaska, submitted to *Tectonics*, 2001]. Of course, the early period of extension in the BBB (Eocene) was more rapid, and may have also been affected by the creation of the Aleutian subduction zone [*Marlow et al.*, 1973; *Scholl et al.*, 1987] or the proposed early-to-mid Eocene subduction of the Kula-Farallon spreading ridge [*James et al.*, 1989; *Plafker and Berg*, 1994].

[79] Regional subsidence began in the late Eocene, as indicated by the onlap of late Eocene basin reflectors onto the red event in the north, and the late Eocene reflectors draping over the horsts in the south (Figures 2 and 3). This subsidence waned from late Oligocene through the middle Miocene as suggested by the decrease in R_r (Figure 5). A possible late Miocene-Holocene increase in subsidence is suggested by a slight increase in R_r. Given that the asymmetry of regional subsidence can be easily modeled in terms of a deflected elastic plate (Figure 8), and that the period of large R_r coincides with a period of voluminous arc volcanism [*Moll-Stalcup*, 1994], we interpret this regional subsidence as due to the deflection of the lithosphere from a major phase of volcanic loading on the Alaska Peninsula. We interpret the high 3–6 km elevation of the apparent volcanic load as a modeling requirement to make up for the effects of an additional parameter(s) or influence(s) not included in the modeling such as (1) regional subsidence associated with fault-controlled extension and subsequent lithospheric cooling (consistent with our interpreted Eocene extension), (2) compression between the North American and Pacific plates [*Cloetingh et al.*, 1989], (3) crustal thickening of the Alaska Peninsula via reverse [*Bond et al.*, 1988] or thrust faulting in the arc, and/or (4) the addition of dense material to the crust via intrusion [*Bond et al.*, 1988].

[80] It is possible that a large component of BBB subsidence is a result of simple N-S extension associated with a lithospheric-scale down-to-the-north normal fault between the Black Hills ridge and the southern boundary of the basin (G. Bond, Columbia University, personal communication, 2003). The BBB horst and graben faults would therefore be considered small antithetic faults within a very large hanging wall. Although we recognize that there is no easy way to distinguish between flexural subsidence due to loading of the arc and regional subsidence expected for a lithospheric-scale half-graben, we do not find evidence that supports this hypothesis from the seismic reflection profile (Figure 1) that was collected over this Black-Hills-ridge fault about 300 km to the west [*Lizarralde et al.*, 2002]. This fault appears to be a major strike-slip fault beneath with a series of minor grabens about 10-km wide, and there is no significant change in crustal properties across the zone [*Lizarralde et al.*, 2002]. In addition, we speculate that if this fault were a lithospheric-scale normal fault that was responsible for the >3 km of Late Eocene-Recent basin subsidence, then the Black Hills ridge would have a much higher elevation since it comprises the footwall over approximately 32-km thick crust [*Fliedner and Klemperer*, 1999, 2000; *Lizarralde et al.*, 2002]. Finally, the Peninsular Terrane probably extends from the mainland toward the southwest beneath the southern Bering Shelf [*McGeary and Ben-Avraham*, 1981; *Cooper et al.*, 1987; *Marlow et al.*, 1987] and therefore creation of a normal fault that cuts through the entire Peninsular Terrane lithosphere would probably require a substantial amount of N-S extension that may be hard to conceive of given the evidence for significant Miocene through Recent arc-perpendicular compression (see Flexural Modeling section; discussion of compression).

[81] The waning of the flexural subsidence in the Miocene roughly correlates with a hiatus in arc volcanism on the

Alaska Peninsula [*Wilson*, 1985; *Scholl et al.*, 1987; *Moll-Stalcup*, 1994]. Furthermore, the possible increase in R_r for the Pliocene-Holocene units correlates with a resurgence of arc volcanism. This renewed Pliocene-Holocene volcanism is probably also the source of the northward prograding deltaic sequences observed in unit A [*Brockway et al.*, 1975; *Turner et al.*, 1988]. The good fit of a 4th-order polynomial curve to the bathymetry profile, and the 30-mGal regional gravity anomaly suggest that flexural subsidence is ongoing (Figure 2, top). In addition, the projected position of Cape Newenham approximately correlates with the predicted flexural bulge for two of the three models (Figure 8), further suggesting ongoing flexural subsidence.

[82] *Worrall* [1991] suggested that the Bristol Bay basin and other outer shelf basins may share the same evolutionary history and subsidence mechanisms (Figure 1). In contrast, *Bond et al.* [1988] suggested that the Bristol Bay basin developed independently from the other outer shelf basins. We interpret the fault-controlled subsidence phase for the Bristol Bay basin as due to extension associated with right-lateral slip along the neighboring strike-slip fault that separates the basin from the Black Hills ridge. Because the Black Hills ridge extends northwest as the Pribilof ridge along the outer Bering Shelf margin, our interpretation implies that there is a genetic relationship between these basins' fault-controlled subsidence. However, our interpretation of BBB regional subsidence as flexural in origin associated with late Eocene-Recent volcanic loading of an active arc (and other factors) implies that this mechanism is unique to the BBB.

[83] A classic "back arc basin" forms at an active margin when extension in the overlying plate causes the arc to rift apart [*Karig*, 1971, 1974]. This spreading continues until both sides of the arc have separated, and subsequent thermal subsidence of the newly created oceanic lithosphere creates accommodation space for the new basin.

[84] A classic "retroarc foreland basin" forms behind the arc of a convergent margin when compression in the overlying plate induces thrust-faulting in the foreland region. This faulting stacks thrust sheets upon one another, loading the lithosphere, deflecting the foreland region, and creating accommodation space for deposition [*Dickinson and Suczek*, 1979].

[85] The Bristol Bay basin (BBB) is a sedimentary basin residing in a back arc setting on continental crust. BBB subsidence appears to have two contributing origins: it has evolved because of both back arc extension and flexure. These characteristics make it different from the classic end-member back arc or retroarc foreland basins. Rather, the BBB is a structural mixture of the two. In that regard, it may be similar to the Taranaki basin, a back arc basin on continental crust along the west coast of New Zealand. The Taranaki basin evolved during the late Cretaceous-Cenozoic in response to episodes of extension, strike-slip faulting, and flexure [*Pilar and Wakefield*, 1978; *Knox*, 1982; *King and Thrasher*, 1992]. All three mechanisms appear to have been controlled by the evolving plate boundary.

[86] The BBB also has similarities to the Andaman Basin. Located behind the Andaman Arc in the east Indian Ocean, the Andaman Basin evolved because of strike-slip-faulting and extension, probably associated with oblique convergence between the Indian and Eurasian plates [*Rodolfo*, 1969; *Curray et al.*, 1979; *Guzman-Speziale and Ni*, 1993; *Lee and Lawver*, 1994]. The degree to which extension is directly related to strike-slip faulting is unclear, but it appears unlikely that steep N-S trending valleys in the western Andaman Sea, some of which appear to be controlled by flanking normal faults [*Rodolfo*, 1969], were created solely by pull-apart tectonics or E-W spreading ridges associated with N-S trending transform faults. Such an ambiguity also exists in the BBB, since back arc extension could be associated with a right-lateral strike-slip faulting or slab rollback. Although both basins are similar in the aforementioned ways, they are quite different in their size and magnitude of structures—the Andaman basin is quite large and deep because seafloor spreading followed rifting.

11. Conclusion

[87] Supported by preexisting geological and geophysical data, we have presented evidence from new geophysical data sets collected during the Pacific to Bering Shelf Deep Seismic Experiment that the Bristol Bay basin (BBB) was created by two different subsidence mechanisms: fault-controlled subsidence and flexural subsidence. We propose that fault-controlled subsidence occurred from the early or middle Eocene through the Miocene, probably associated with slip along a major right-lateral strike-slip fault that separates the BBB from the Black Hills ridge toward the southwest. Flexural subsidence began in the late Eocene because of volcanic loading of the arc, and was amplified by a combination of thermal cooling of the lithosphere (subsequent to prior extension), tectonic compression, reverse or thrust faulting on the Alaska Peninsula, and/or the intrusion of dense material to the upper crust in the back arc. We suggest that flexural subsidence decreased through the early Miocene, then stayed constant (or possibly increased) through the Holocene in response to arc volcanism and the northward progradation of a deltaic sequence. The two subsidence mechanisms suggest that the evolution of the BBB has components typically found in both back arc (extension) and retroarc foreland (flexure) basins.

[88] Recent studies have shown that the Pacific hot spots have not remained fixed relative to other hot spots [*Raymond et al.*, 2000; *Steinberger and O'Connell*, 2000]. As a result, the 43-Ma bend in the Hawaiian-Emperor seamount chain is now ambiguous. Either the motion of the Pacific plate with respect to a fixed mantle changed direction and/or speed, and/or the drift of the Hawaiian hot spot changed its direction and/or speed. In addition, there is a great deal of ambiguity as to the location and spreading history of the Kula/Farallon and Kula/Pacific spreading ridges [*DeLong and Fox*, 1977; *Jackson et al.*, 1978; *Byrne*, 1979; *Engebretson et al.*, 1985; *James et al.*, 1989; *Plafker and Berg*, 1994]. Further work to constrain the tectonic evolution of the Bristol Bay basin will depend, in part, on ongoing work to solve these important problems.

[89] **Acknowledgments.** There were many individuals who helped make this work possible. We wish to thank John Diebold for the sonobuoy refraction velocity data, Rick Saltus for an isostasy gravity data set of Alaska, Steve Holbrook for the far-field signature of the R/V Ewing's airgun array, and Joyce Alsop for her tireless efforts in locating various archived data at Lamont Doherty Earth Observatory. We also wish to thank John Madsen, Dick Benson, Norm Sleep, and Dave Scholl for their advice and support, and the Captain, crew, and Shipboard Scientific Party of R/V *Ewing* cruise EW94-09, together with Steve Holbrook (University of Wyoming), Moritz Fliedner (3DGeo Development Inc.), and Dan Lizarralde (Georgia Tech) for their hard work during the Pacific to Bering Shelf Deep Seismic Experiment. We also thank the National Science Foundation, the University of Delaware Undergraduate Research Program, the University of Delaware Department of Geology, and Stanford University Department of Geophysics for their financial support throughout this research. Finally, we thank C. H. Jones and G. Bond for their constructive reviews of this manuscript.

References

Bailey, D. K., A. K. Cooper, M. S. Marlow, and D. S. Scholl, Preliminary residual magnetic map of the Bering shelf and parts of Alaska, scale 1:2,500,000, *U.S. Geol. Surv. Misc. Field Stud. Map, MF-716*, 1976.

Barnes, D. F., J. Marino, R. L. Morin, C. W. Roberts, and R. C. Jachens, Incomplete isostatic gravity map of Alaska, in *The Geology of North America*, vol. G-1, *The Geology of Alaska*, edited by G. Plafker and H. C. Berg, Geol. Soc. of Am., Boulder, Colo., 1994.

Beikman, H. M., Geologic Map of Alaska, scale 1:2,500,000, U.S. Geol. Surv., 1980.

Bond, G. C., S. D. Lewis, J. Taber, M. S. Steckler, and M. A. Kominz, Evidence for formation of a flexural back arc basin by compression and crustal thickening in the central Alaska Peninsula, *Geology*, *16*, 1147–1150, 1988.

Brockway, R. G., B. Alexander, P. Day, W. Lyle, R. Hiles, W. Decker, W. Polshi, and B. Reed, Bristol Bay region stratigraphic correlation section, southwest Alaska, Alaska Geol. Soc., Anchorage, 1975.

Burger, H. R., *Exploration Geophysics*, 489 pp., Prentice Hall, Old Tappan, N. J., 1992.

Burk, C. A., Geology of the Alaska Peninsula island arc and continental margin, *Mem. Geol. Soc. Am.*, *99*, 250 pp., 1965.

Byrne, T., Late Paleocene demise of the Kula-Pacific spreading center, *Geology*, *7*, 341–344, 1979.

Childs, J. R., A. K. Cooper, and A. W. Wright, Residual magnetic map of Umnak Plateau region, southeastern Bering Sea, scale 1:1,000,000, *U.S. Geol. Surv. Geol. Invest. Map, GP-939*, 1981.

Childs, J. R., H. W. Magistrale, and A. K. Cooper, Free-air gravity anomaly map of the Bering Sea, scale 1:2,500,000, *U.S. Geol. Surv. Misc. Field Stud. Map, MF-1728*, 1985.

Cloetingh, S., H. Kooi, and W. Groenewoud, Intraplate stresses and sedimentary basin evolution, in *Origin and Evolution of Sedimentary Basins and Their Energy and Mineral Resources*, *Geophys. Monogr. Ser.*, vol. 48, edited by R. A. Price, pp. 1–16, AGU, Washington, D. C., 1989.

Cooper, A. K., and M. S. Marlow, Deep water basins of the Bering Sea: Tectonics and hydrocarbon potential, *J. Alaska Geol. Soc.*, *3*, 57–58, 1983.

Cooper, A. K., and M. S. Marlow, Geophysical and geological studies of the Bering Sea shelf, in *United States Geological Survey in Alaska: Accomplishments During 1982*, edited by K. M. Reed and W. S. Bartsch, *U.S. Geol. Surv. Circ., 0939*, 123–127, 1984.

Cooper, A. K., M. S. Marlow, A. W. Parker, and H. R. Childs, Structure contour map on acoustic basement in the Bering Sea, scale 1:2,500,000, *U.S. Geol. Surv. Misc. Field Stud. Map, MF-1165*, 1979.

Cooper, A. K., M. S. Marlow, and D. W. Scholl, Multifold seismic data across outer Bering Sea continental margin (abstract), *AAPG Bull.*, *64*, 694, 1980.

Cooper, A. K., M. S. Marlow, and D. W. Scholl, Geologic framework of the Bering Sea crust, in *Geology and Resource Potential of the Continental Margin of Western North America and Adjacent Ocean Basins, Beaufort Sea to Baja California*, edited by D. W. Scholl, A. Grantz, and J. G. Vedder, pp. 73–102, Circum-Pac. Counc. for Energy and Miner. Resour., Houston, Tex., 1987.

Curray, J. R., D. G. Moore, L. A. Lawver, F. J. Emmel, R. W. Raitt, M. Henry, and R. M. Kieckhefer, Tectonics of the Andaman Sea and Burma, in *Geological and Geophysical Investigations of Continental Margins*, edited by J. Watkins, L. Montadert, and P. W. Dickerson, *AAPG Mem., 29*, 189–198, 1979.

Decker, J., et al., Geology of southwestern Alaska, in *The Geology of North America*, vol. G-1, *The Geology of Alaska*, edited by G. Plafker and H. C. Berg, pp. 285–310, Geol. Soc. of Am., Boulder, Colo., 1994.

DeLong, S. E., and P. J. Fox, Geological consequences of ridge subduction, in *Island Arcs, Deep Sea Trenches and Back-Arc Basins*, *Maurice Ewing Ser.*, vol. 1, edited by M. Talwani and W. C. Pitmann III, pp. 221–228, AGU, Washington, D. C., 1977.

Detterman, R. L., T. P. Miller, M. E. Yount, and F. H. Wilson, Geologic map of the Chignik and Sutwik Island quadrangles, Alaska, scale 1:250,000, *U.S. Geol. Surv. Misc. Invest. Map, I-1229*, 1981.

Dickinson, W. R., and C. A. Suczek, Plate tectonics and sandstone compositions, *AAPG Bull.*, *63*, 2164–2182, 1979.

Engebretson, D. C., A. Cox, and R. G. Gordan, Relative motions between oceanic and continental plates in the Pacific basin, *Spec. Pap. Geol. Soc. Am.*, *206*, 59 pp., 1985.

Fliedner, M. M., and S. L. Klemperer, Composition of an island-arc: Wide-angle studies in the eastern Aleutian islands, Alaska, *J. Geophys. Res.*, *59*, 10,667–10,694, 1999.

Fliedner, M. M., and S. L. Klemperer, Crustal structure transition from oceanic arc to continental arc, eastern Aleutian Islands and Alaska Peninsula, *Earth Planet. Sci. Lett.*, *179*, 567–579, 2000.

Guzman-Speziale, M., and J. F. Ni, The opening of the Andaman Sea: Where is the short-term displacement being taken up?, *Geophys. Res. Lett.*, *20*, 2949–2952, 1993.

Hanks, T. C., The Kuril trench-Hokkaido rise system: Large shallow earthquakes and simple models of deformation, *Geophys. J. R. Astron. Soc.*, *23*, 173–189, 1971.

Haq, B. U., J. Hardenbol, and P. R. Vail, Chronology of fluctuating sea levels since the Triassic, *Science*, *235*(4793), 1156–1167, 1987.

Hatten, C. W., Petroleum potential of Bristol Bay basin, Alaska, in *Future Petroleum Provinces of the United States: Their Geology and Potential*, vol. 1, *AAPG Mem.*, *15*, 105–108, 1971.

Holbrook, W. S., D. Lizarralde, S. McGeary, N. Bangs, and J. Diebold, Structure and composition of the Aleutian island arc and implications for continental crustal growth, *Geology*, *27*, 31–34, 1999.

Jackson, E. D., et al., Off Hawaii, drilling confirms hot spot origins, *Geotimes*, *23*, 23–26, 1978.

James, T. S., L. S. Hollister, and W. J. Morgan, Thermal modeling of the Chugach metamorphic complex, *J. Geophys. Res.*, *94*, 4411–4423, 1989.

Jin, D. J., and E. Herrin, Surface wave studies of the Bering Sea and Alaska area, *Bull. Seismol. Soc. Am.*, *67*, 2117–2144, 1980.

Jin, Y., M. K. McNutt, and Y. Zhu, Mapping the descent of Indian and Eurasian plates beneath the Tibetan Plateau from gravity anomalies, *J. Geophys. Res.*, *101*, 1275–1290, 1996.

Jones, D. L., and N. J. Silberling, Mesozoic stratigraphy: The key to tectonic analysis of southern and central Alaska, *U.S. Geol. Surv. Open File Rep., 79-1200*, 41 pp., 1979.

Jordan, T. E., Thrust loads and foreland basin evolution, Cretaceous, western United States, *APG Bull.*, *65*, 2506–2520, 1981.

Karig, D. E., Origin and development of marginal basins, *J. Geophys. Res.*, *76*, 2543–2561, 1971.

Karig, D. E., Evolution of arc systems in the western Pacific, *Annu. Rev. Earth Planet. Sci.*, *2*, 51–75, 1974.

Karner, G. D., and A. B. Watts, Gravity anomalies and flexure of the lithosphere at mountain ranges, *J. Geophys. Res.*, *88*, 10,449–10,477, 1983.

King, P. R., and G. P. Thrasher, Post-Eocene development of the Taranaki Basin, New Zealand, Convergent overprint of a passive margin, in *Geology and Geophysics of Continental Margins*, edited by J. S. Watkins, F. Zhiqiang, and K. J. McMillan, *AAPG Mem.*, *53*, 73–118, 1992.

Klemperer, S. L., E. L. Miller, A. Grantz, D. W. Scholl, and the Bering-Chukchi Working Group, Crustal structure of the Bering and Chukchi shelves: Deep seismic reflection profiles across the North American continent between Alaska and Russia, in *Tectonic Evolution of the Bering Shelf-Chukchi Sea-Arctic Margin and Adjacent Landmasses*, edited by E. L. Miller, A. Grantz, and S. L. Klemperer, *Spec. Pap. Geol. Soc. Am.*, *360*, 1–24, 2002.

Knox, G. J., Taranaki Basin, Structural style and tectonic setting, *N. Z. J. Geol. Geophys.*, *25*, 125–140, 1982.

Lee, T. Y., and L. A. Lawver, Cenozoic plate reconstruction of the South China Sea region, *Tectonophysics*, *235*, 149–180, 1994.

Liou, J. G., Y. Seki, R. N. Guillemette, and H. Sakai, Phase equilibria and mixed parageneses of metabasites in low-grade metamorphism, in *Diagenesis and Low-Temperature Metamorphism*, edited by D. Robinson, *Mineral. Mag.*, *49*(352), 321–333, 1985.

Lizarralde, D., W. S. Holbrook, S. McGeary, N. L. Bangs, and J. B. Diebold, Crustal construction of a volcanic arc, wide-angle seismic results from the western Alaska Peninsula, *J. Geophys. Res.*, *107*(B8), 2164, 10.1029/2001JB000230, 2002.

Lyon-Caen, H., and P. Molnar, Constraints on the structure of the Himalaya from an analysis of gravity and a flexural model of the lithosphere, *J. Geophys. Res.*, *88*, 8171–8192, 1983.

Marlow, M. S., and A. K. Cooper, Mesozoic and Cenozoic structural trends under southern Bering Sea shelf, *AAPG Bull.*, *64*, 2139–2155, 1980.

Marlow, M. S., D. W. Scholl, E. C. Buffington, and T. R. Alpha, Tectonic history of the central Aleutian Arc, *Geol. Soc. Am. Bull.*, *84*, 1555–1574, 1973.

Marlow, M. S., D. W. Scholl, A. K. Cooper, and E. C. Buffington, Structure and evolution of Bering Sea shelf south of St. Lawrence Island, *AAPG Bull.*, *60*, 161–183, 1976.

Marlow, M. S., D. W. Scholl, and A. K. Cooper, St. George Basin, Bering Sea Shelf: A collapsed Mesozoic margin, in *Island Arcs, Deep Sea Trenches, and Back-Arc Basins*, *Maurice Ewing Ser.*, vol. 1, edited by M. Talwani and W. C. Pitman III, pp. 211–220, AGU, Washington, D. C., 1977.

Marlow, M. S., A. K. Cooper, and M. A. Fisher, Petroleum geology, Beringian continental shelf, in *Geology and Resource Potential of the Continental Margin of Western North America and Adjacent Ocean Basins, Beaufort Sea to Baja California*, edited by D. W. Scholl, A. Grantz, and J. G. Vedder, pp. 103–122, Circum-Pac. Counc. for Energy and Miner. Resour., Houston, Tex., 1987.

Marlow, M. S., A. K. Cooper, and M. A. Fisher, Geology of the eastern Bering Sea continental shelf, *The Geology of North America*, vol. G-1, *The Geology of Alaska*, edited by G. Plafker and H. C. Berg, pp. 271–284, Geol. Soc. of Am., Boulder, Colo., 1994.

McGeary, S., and Z. Ben-Avraham, Allochthonous terranes in Alaska: Implications for the structure and evolution of the Bering Sea shelf, *Geology*, *9*, 608–614, 1981.

McGeary, S., J. B. Diebold, N. L. Bangs, G. Bond, and P. Buhl, Preliminary results of the Pacific to Bering shelf deep seismic experiment (abstract), *Eos. Trans. AGU*, *75*(44), Fall Meet. Suppl., 643, 1994.

McKenzie, D., Some remarks on the development of sedimentary basins, *Earth Planet. Sci. Lett.*, *40*, 25–32, 1978.

McLean, H., Organic geochemistry, lithology, and paleontology of Tertiary and Mesozoic rocks from wells on the Alaska Peninsula, *U.S. Geol. Surv. Open File Rep., 77-0813*, 68 pp., 1977.

Moll-Stalcup, E. J., Geology of west-central Alaska, *The Geology of North America*, vol. G-1, *The Geology of Alaska*, edited by G. Plafker and H. C. Berg, pp. 241–269, Geol. Soc. of Am., Boulder, Colo., 1994.

Niazi, M., and K. Chun, Crustal structure in the southern Bering shelf and the Alaska Peninsula from inversion of surface-wave dispersion data, *Bull. Seismol. Soc. Am.*, *79*, 1883–1893, 1989.

Pilar, W. F. H., and L. I. Wakefield, Structural and stratigraphic evolution of the Taranaki Basin, offshore North Island, New Zealand, *APPEA J.*, *18*, 93–101, 1978.

Plafker, G., and H. C. Berg, Overview of the geology and tectonic evolution of Alaska, *The Geology of North America*, vol. G-1, *The Geology of Alaska*, edited by G. Plafker and H. C. Berg, pp.. 989–1021, Geol. Soc. of Am., Boulder, Colo., 1994.

Plafker, G., W. J. Nokleberg, and J. S. Lull, Summary of the 1984 TACT geologic studies in the northern Chugach Mountains and southern Copper River basin, *U.S. Geol. Surv. Circ.*, *967*, 76–79, 1985.

Pratt, R. M., M. S. Rutstein, W. F. Walton, and J. A. Buschur, Extension of Alaska structural trends beneath Bristol Bay, Bering shelf, Alaska, *J. Geophys. Res.*, *77*, 4994–4999, 1972.

Raymond, C. A., J. M. Stock, and S. C. Cande, Fast Paleogene motion of the Pacific hot spots from revised global plate circuit constraints, in *The History and Dynamics of Global Plate Motions*, *Geophys. Monogr. Ser.*, vol. 121, edited by M. A. Richards, R. Gordon, and R. D. van der Hilst, pp. 359–375, AGU, Washington, D. C., 2000.

Rodgers, D. A., Sedimentation in oblique-slip mobile zones, in *Special Publication of the International Association of Sedimentologists*, edited by P. F. Ballance and H. G. Reading, pp. 27–41, Blackwell, Malden, Mass., 1980.

Rodolfo, K. S., Bathymetry and marine geology of the Andaman Basin, and tectonic implications for Southeast Asia, *Geol. Soc. Am. Bull.*, *80*, 1203–1230, 1969.

Scholl, D. W., T. L. Vallier, and A. J. Stevenson, Geologic evolution and petroleum geology of the Aleutian Ridge, in *Geology and Resource Potential of the Continental Margin of Western North America and Adjacent Ocean Basins, Beaufort Sea to Baja California*, edited by D. W. Scholl, A. Grantz, and J. G. Vedder, pp. 73–102, Circum-Pac. Counc. for Energy and Miner. Resour., Houston, Tex., 1987.

Sheffels, B., and M. McNutt, Role of subsurface loads and regional compensation in the isostatic balance of the Transverse Ranges, California: Evidence for intracontinental subduction, *J. Geophys. Res.*, *91*, 6419–6431, 1986.

Steinberger, B., and R. J. O'Connell, Effects of mantle flow on hot spot motion, in *The History and Dynamics of Global Plate Motions*, *Geophys. Monogr. Ser.*, vol. 121, edited by M. A. Richards, R. Gordon, and R. D. van der Hilst, pp. 377–398, AGU, Washington, D. C., 2000.

Turner, R. F., C. M. McCarthy, M. B. Lynch, P. J. Hoose, G. C. Martin, J. A. Larson, T. O. Flett, K. W. Sherwood, and A. J. Adams, Geological and operational summary, North Aleutian Shelf COST No. 1 Well, Bering Sea, Alaska, 256 pp., U.S. Dep. of the Inter. Miner. Manage. Serv., Alaska OCS Reg., Anchorage, 1988.

Walcott, R. I., Flexure of the lithosphere at Hawaii, *Tectonophysics*, *9*, 435–446, 1970.

Walker, K. T., The evolution of the Bristol Bay basin: Evidence from geophysical data, B. S. thesis, 150 pp., Univ. of Del., Newark, 1998.

Watts, A. B., An analysis of isostasy in the world's oceans: 1. Hawaiian-Emperor Seamount Chain, *J. Geophys. Res.*, *83*, 5989–6004, 1978.

Watts, A. B., and J. R. Cochran, Gravity anomalies and flexure of the lithosphere along the Hawaiian-Emperor Seamount Chain, *Geophys. J. R. Astron. Soc.*, *38*, 119–141, 1974.

Watts, A. B., and M. Talwani, Gravity anomalies seaward of deep-sea trenches and their tectonic implications, *Geophys. J. R. Astron. Soc.*, *36*, 57–90, 1974.

Wilson, F. H., Meshik and Aleutian arcs: Tertiary volcanism on Alaska Peninsula, Alaska (abstract), *AAPG Bull.*, *69*, 683, 1985.

Wilson, F. H., J. E. Case, and R. L. Detterman, Preliminary description of a Miocene zone of structural complexity, Port Moller and Stepovak Bay quadrangles, in the United States Geological Survey in Alaska: Accomplishments During 1983, *U.S. Geol. Surv. Circ.*, *954*, 55–56, 1983.

Worrall, D. M., Tectonic history of the Bering Sea and the evolution of the Tertiary strike-slip basins of the Bering Shelf, *Spec. Pap. Geol. Soc. Am., 257*, 120 pp., 1991.

S. L. Klemperer, Department of Geophysics, Stanford University, Stanford, CA 94305, USA. (sklemp@stanford.edu)

S. E. McGeary, Department of Geology, University of Delaware, Newark, DE 19716, USA. (smcgeary@udel.edu)

K. T. Walker, Department of Geophysics, Stanford University, Mitchell Building, Stanford, CA 94305-2215, USA. (ktwalker@pangea.stanford.edu)